UNIVERSIDAD DE CHILE

FACULTAD DE CIENCIAS QUÍMICAS Y FARMACÉUTICAS

Escuela de Postgrado

Angiotensin-(1-9) prevents cardiomyocyte hypertrophy via miR-129-3p/PKIA/PKA signaling pathway

Cristian Sotomayor Flores

Ph.D, in Biochemistry, Universidad de Chile, Chile

Ph.D. in Natural Sciences, Universität Regensburg, Germany

Dr. Sergio Lavandero

Universidad de Chile

Dr. Alejandro Corvalán

P. Universidad Católica de Chile

Dr. Gunter Meister

Universität Regensburg

UNIVERSIDAD DE CHILE
FACULTAD DE CIENCIAS QUÍMICAS Y FARMACÉUTICAS

INFORME DE APROBACIÓN DE TESIS DE DOCTORADO

Se informa a la Dirección de la Escuela de Graduados de la Facultad de Ciencias Químicas y Farmacéuticas que la Tesis de Doctorado presentada por el candidato:

Cristian Sotomayor Flores

Ha sido aprobada por la Comisión de Evaluadora de Tesis como requisito para optar al grado de Doctor en Bioquímica, en el examen público rendido el día _____

Directores de Tesis:

Dr. Sergio Lavandero   _____

Dr. Alejandro Corvalan   _____

Comisión Evaluadora de Tesis:

Dr. Lee Meisel (Presidenta)   _____

Dr. Ramón Rodrigo   _____

Dr. Alvaro Glavic   _____

Dr. Xavier Figueroa   _____

AGRADECIMIENTOS

FINANCIAMIENTO

PUBLICACIONES Y DIFUSIÓN DEL CONOCIMIENTO:

Publicaciones

- **Sotomayor-Flores C**, Rivera-Mejías P, Vásquez-Trincado C, et al. Angiotensin-(1-9) prevents cardiomyocyte hypertrophy by controlling mitochondrial dynamics via miR-129-3p/PKIA pathway [published online ahead of print, 2020 Mar 9]. Cell Death Differ. 2020; doi:10.1038/s41418-020-0522-3, PMID: 32152556. **ISI: 8,1** Top 10 journal (RNK 27/299).

- Peña-Oyarzun D, Rodriguez-Peña M, Burgos-Bravo F, Vergara A, Kretschmar C, **Sotomayor-Flores C**, Ramirez-Sarmiento C, Smedt H, Reyes M, Perez W, Torres V, Moreselli E, Altamirano F, Wilson C, Hill J, Lavandero S, Criollo A. PKD2/polycystin-2 induces autophagy by forming a complex with BECN11. Autophagy. 2020 June 30 doi: 10.1080/15548627.2020.1782035. **ISI 11,1**. Top 10 journal (RNK 14/193). PMID: 32543276

- Criollo A, Altamirano F, Pedrozo Z, Schiattarella GG, Li DL, Rivera-Mejías P, **Sotomayor-Flores C**, Parra V, Villalobos E, Battiprolu PK, Jiang N, May HI, Morselli E, Somlo S, de Smedt H, Gillette TG, Lavandero S, Hill JA. Polycystin-2-dependent control of cardiomyocyte autophagy. **Journal Molecular Cellular Cardiology**. 2018; 118:110-121. PMID: 29518398

- Oyarzún AP, Westermeier F, Pennanen C, López-Crisosto C, Parra V, **Sotomayor-Flores C**, Sánchez G, Pedrozo Z, Troncoso R, Lavandero S. FK866 compromises mitochondrial metabolism and adaptive stress responses in cultured cardiomyocytes. Biochemical Pharmacology. 2015; 98:92-101. PMID: 26297909

- Gutiérrez T, Parra V, Troncoso R, Pennanen C, Contreras-Ferrat A, Vasquez-Trincado C, Morales PE, Lopez-Crisosto C, **Sotomayor-Flores C**, Chiong M, Rothermel BA, Lavandero S. Alteration in mitochondrial Ca(2+) uptake disrupts insulin signaling in hypertrophic cardiomyocytes. **Cell Communication Signaling**. 2014 Nov 7; 12:68. doi: 10.1186/s12964-014-0068-4. PMID: 25376904

- Morales PE, Torres G, **Sotomayor-Flores C**, Peña-Oyarzún D, Rivera-Mejías P, Paredes F, Chiong M. GLP-1 promotes mitochondrial metabolism in vascular smooth muscle cells by enhancing endoplasmic reticulum-mitochondria coupling. **Biochemical Biophysical Research Communications**. 2014; 446:410-6. PMID: 24613839

- Carrasco L, Cea P, Rocco P, Peña-Oyarzún D, Rivera-Mejias P, **Sotomayor-Flores C**, Quiroga C, Criollo A, Ibarra C, Chiong M, Lavandero S. <u>Role of heterotrimeric G protein and calcium in cardiomyocyte hypertrophy induced by IGF-1.</u> **Journal Cellular Biochemistry** 2014; 115:712-20. PMID: 24243530

- Carrasco L, Cea P, Rocco P, Peña-Oyarzún D, Rivera-Mejias P, **Sotomayor-Flores C**, Quiroga C, Criollo A, Ibarra C, Chiong M, Lavandero S. Role of heterotrimeric G protein and calcium in cardiomyocyte hypertrophy induced by IGF-1. **Journal Cellular Biochemistry** 2014;115:712-20. PMID: 24243530

Presentaciones a congresos nacionales e internacionales

- **Sotomayor Flores C**, Rivera Mejías P, Morales P, López-Crisosto C, Jalil JE, Ocaranza MP, Chiong M, Parra V, Lavandero S. Angiotensin-(1-9) regulates cardiomyocyte mitochondrial calcium by AT2 receptor. XXXVII Reunión anual sociedad Bioquímica y biología molecular. 30.09.2014-04.10.2014. Puerto Varas. Chile.

- **Sotomayor Flores C,** Rivera Mejías P, Novel insights of Angiotensin-(1-9). Expositor for visit and collaboration program between Department of Physiology and Biophysics, Institute of Biological Sciences, Universidade Federal de Minas Gerais, Belo Horizonte, Brazil and Advanced Center for Chronic Diseases 12-13.11.2014

- **Sotomayor Flores C**, Lavandero S, miRNA expression pattern induced by Ang- (1-9) and its relationship with cardiac hypertrophy. Analysis of NextGen RNA-Seq data for expression profiling and protein-binding RNAs 10-14.10.2016 |Graduate Research Academy. RNA Biology, Germany. Regensburg Germany.

Estadías de investigación en el extranjero:

- **2015.** Biochemistry Center Regensburg (BZR), Laboratory for RNA Biology, University of Regensburg, Regensburg, Germany **(11.02.2015-10.28.2016)**

- **2018** Biochemistry Center Regensburg (BZR), Laboratory for RNA Biology, University of Regensburg, Regensburg, Germany **(3 Months)**

- **2019** Biochemistry Center Regensburg (BZR), Laboratory for RNA Biology, University of Regensburg, Regensburg, Germany **(1 Month)**

Cursos

- Method Course. Transcriptomic with RNA-seq. R programing and RNA-seq analysis. 04-08.04.2016| & 10-14.10.2016. Regensburg. Germany.

LIST OF ABBREVIATIONS

ACE   Angiotensin Converting Enzyme

ACE2   Angiotensin Converting Enzyme type 2

Ang II   Angiotensin II

Ang-(1-9)   Angiotensin-(1-9)

ANP   Atrial Natriuretic Peptide

ANS   Adrenergic Nervous System

AT1R   Angiotensin II receptor type 1

AT2R   Angiotensin II receptor type 2

BNP   Brain Natriuretic Peptide

CaMK   Calmodulin Kinase

CARL   Cardiac Apoptosis Related Long non-coding RNAs

CHRF   Cardiac hypertrophy related Factor

CICR   Calcium induced, calcium release

DAG   Diacylglicerol

DNMTs   DNA Methyltransferases

Drp-1   Dynamin Related Protein-1

ER   Endoplasmic Reticulum

FIS   Fission Protein

HDAC	Histone Deacetylase
IP3	Inositol triphosphate
lncRNAs	Long non-coding RNAs
LTCC	L Type Calcium Channels
MAPK	Mitogen Activated Protein Kinases
MBD	Methyl Binding Proteins
MEF2	Myocyte Enhancer Factor 2
MFN	Mitofusin Protein
miRNAs	micro RNAs
MREs	miRNA response elements
ncRNAs	Non-coding RNAs
NCX	Na+/Ca2+ exchanger
NE	Norepinephrine
NEP	Neutral Endopeptidase
NFAT	Nuclear Factor of activated T cells
NO	Nitric Oxide
OPA	Optic Atrophy Protein
PKA	Protein Kinase A
PKA	Protein Kinase A
PKC	Protein Kinase C

PKIA	Protein Kinase A (inhibitor)
PLC	Phospholipase C
PLN	Phospholamban protein
RAS	Renin Angiotensin System
RISC	RNA-induced silencing complex
ROS	Reactive Oxygen Species
RyR	Ryanodine Receptor
SERCA	Sarco/Endoplasmic reticulum Ca2+-ATPase
STZ	Streptozotocin
TAC	Transverse Aortic Constriction

LIST OF FIGURES

Sapere Aude!

Memento, homo,

quia pulvis es,

et in pulverem reverteris

Contents

ABSTRACT

Angiotensin-(1-9) is a peptide from the non-canonical renin-angiotensin system with anti-hypertrophic effects in cardiomyocytes via an unknown mechanism. Our previous work proved that this peptide induces mitochondrial fusion through Drp1 phosphorylation and prevented norepinephrine-elicited mitochondrial fission.

In the present work, we aimed to elucidate the underlying mechanism by which angiotensin-(1-9) could prevent cardiomyocyte hypertrophy together with its effects over mitochondrial dynamics evaluating the possible link between them and the signaling pathways activated during hypertrophy.

Here we show, for the first time, that angiotensin-(1-9) prevents intracellular calcium dysregulation and the activation of Calcineurin/NFAT signaling pathway at a transcription and protein level in a model of norepinephrine-induced cardiomyocyte hypertrophy. To further investigate the anti-hypertrophic mechanism of angiotensin-(1-9), we performed RNA-seq studies, identifying the upregulation of miR-129 under angiotensin-(1-9) treatment. miR-129 decreased the transcript levels of the protein kinase A inhibitor (PKIA), resulting in the activation of the protein kinase A (PKA) signaling pathway. Finally, we showed that the mere activation of PKA by angiotensin-(1-9) accounted for its effects on calcium handling and cardiomyocyte hypertrophy.

INTRODUCTION

1.1. Cardiovascular system

The cardiovascular system consists of three components: the heart, the blood, and the blood vessels. The heart behaves as a hydraulic pump, creating the driving force behind the pulsatile blood flow through the arterial system. In contrast, the systemic circulatory system acts as a parallel circuit, and the distribution of blood to each of the body organs varies, depending on the relative resistance of the arterioles and capillaries preceding the organ system. The heart is enclosed within the pericardium, a thin but tough connective tissue sheath that provides protection and anchoring of the cardiac tissue within the chest cavity, as well as acts as a constraint that prevents the overfilling of the heart chambers. The heart muscle is made up of cardiac muscle cells (cardiomyocytes) connected by intercalated discs. The arteries move blood away from the heart and, except for the pulmonary artery, carry oxygenated blood. The capillaries are thin-walled and form the site of gas exchange within the tissues (1).

1.1.1. Cellular composition of the heart:

The heart is composed of cardiomyocytes, non-myocytes (fibroblasts, endothelial cells, mast cells, and vascular smooth muscle cells) and the surrounding extracellular matrix. Ventricular cardiomyocytes makeup only one-third of total cell number, but account for around 70% of the heart mass (2):

Cardiomyocytes. They are the contractile units of the heart. These cells are composed of myofibrils, containing myofilaments, which consists of sarcomeres, the basic contractile unit of the heart. Cardiomyocytes are arranged in a circumferential and spiral orientation around the left ventricle and need to contract simultaneously to ensure the heart pumps with a regular rhythm. Intercalated discs, located at the bipolar ends of cardiomyocytes, are responsible for maintaining cell-cell adhesion

while allowing contractile force to be transmitted between adjacent cardiomyocytes (3)

Non-myocytes. Non-muscle cells constitute approximately 65--70% of the heart. The non-myocytes cells are endothelial cells, fibroblasts, pericytes, smooth muscle cells, and macrophages. The endothelial cells lining the internal wall of the ventricle possess different surface, morphology, and shape than those lined with blood vessels. Fibroblasts are mostly scattered among the cardiac muscle cells, and they contain highly developed rough-surfaced endoplasmic reticulum along with other structural features. Pericytes are characteristically observed on the periphery of the blood vessels and they show structural similarities to the fibroblasts. Smooth muscle cells are relatively fewer than other non-muscle cells and generally serve to line the wall of the medium caliber blood vessels of the heart. Although macrophages are observed in different regions of the heart, a small number of macrophage-like cells are firmly attached to the surfaces of the cardiac muscle cells. Macrophages are mainly identified with their abundant filopodia, lysosomes, and lysosomal degradation products (2). Cardiac fibroblasts and cardiac endothelial cells form the majority of these non-myocyte cells. Cardiac fibroblasts serve a structural role by providing the extracellular matrix of the heart, mechanotransduction cues, and paracrine factors that regulate cardiomyocyte maturation, whilst cardiac endothelial cells form the myocardial microvasculature, which governs the supply of oxygen and free fatty acids to the cardiomyocytes. Cardiac endothelial cells also release paracrine factors that regulate cardiomyocyte metabolism, survival, and contractile function (4)

1.1.2. Regulation of cardiovascular system

Adrenergic Nervous System (ANS). The ANS exerts a wide variety of cardiovascular effects, including heart rate acceleration (positive chronotropy), an increase in cardiac contractility (positive inotropy), accelerated cardiac relaxation (positive lusitropy), decrease in venous capacitance and constriction of resistance

and cutaneous vessels. All these effects aim to increase cardiac performance to prepare and enable the body for the so-called "fight or flight response." Conversely, the mirror branch of the autonomic nervous system, the parasympathetic (cholinergic) nervous system, slows the heart rate (bradycardia) through vagal nerve impulses, with minimal or no effect on cardiac contractility. This is because the ventricles, whose contraction is responsible for pumping the blood into the systemic and pulmonary circulations, receive almost exclusively adrenergic fiber innervations. In contrast, the cholinergic system fibers run with the vagus nerve subendocardially, after it crosses the atrioventricular groove, and reach mainly the atrial myocardium with minimal connections to the ventricular myocardium (5).

Renin-angiotensin system (RAS). RAS plays a crucial role in cardiovascular and hydro electrolyte homeostasis. The formation of the biologically active end-products of this peptide hormonal system is dependent on a limited proteolysis process starting with the cleavage of precursor, the glycoprotein angiotensinogen, by renin. This step occurs in the circulation but also in many organs and tissues. The formation of the octapeptide angiotensin II (Ang-(1-8) or Ang II) from angiotensin I (Ang-(1-10) or Ang I), the product of angiotensinogen hydrolysis by renin, is mainly dependent of angiotensin converting enzyme (ACE), a dipeptidyl carboxyl-peptidase that is widely expressed in many tissues including in the endothelium, a strategic localization for the formation of circulating Ang II (6). RAS has been traditionally defined as a circulating, endocrine system, which exerts its role through the action of the effector peptide, angiotensin II on its receptor. Circulating Ang II affects multiple organs: It is responsible for systemic vasoconstriction, adrenal aldosterone release, hypophyseal vasopressin secretion, and renal sodium reabsorption. It also affects cardiac parameters such as preload and afterload, as well as short-term cardiac homeostasis (7). In the early 1970s, the major components of 'classical' circulating RAS **(Fig. 1)** were identified, and there was compelling evidence to indicate important roles for RAS in the regulation of fluid balance and blood pressure. At that time, however, there was widespread skepticism regarding the role of RAS in cardiovascular disease. It was not until the discovery of orally active ACE

inhibitors, the first of which was captopril, that the paramount importance of RAS in cardiovascular homeostasis and disease was being appreciated. The introduction of losartan, the first orally active and effective angiotensin receptor type 1 (ATR1) blocker further strengthened this concept (8)
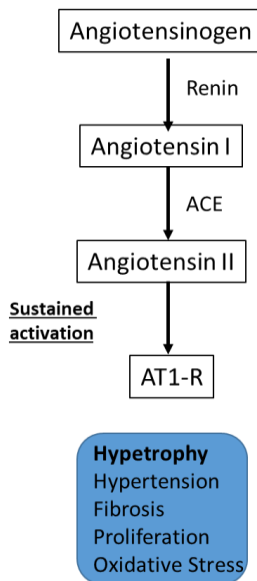
Fig. 1. A simplified view of the classic renin angiotensin system (RAS). Renin carries out the conversion of angiotensinogen to angiotensin I, which is subsequently converted to angiotensin II by the angiotensin-converting enzyme (ACE). Angiotensin II through the interaction with its receptor AT1-R can induce blood vessels to narrow, increasing blood pressure and stimulate the secretion of aldosterone, to increase the reabsorption of sodium and water. The sustained activation of this system could cause hypertension, hypertrophy, fibrosis, proliferation of non-myocytes and Oxidative stress within the cardiovascular system. Adapted from Fyhrquist et al. Renin-angiotensin system revisited. J Intern Med. 2008;264:224–34

However, the RAS system is a more complex system than initially thought. In addition to Ang II, other biologically active end-products can be formed, including Ang III, Ang IV, Ang A, and Alamandine through the action of different enzymes like prolyl-endopeptidase, neutral-endopeptidase (NEP), and tymeth-oligopeptidase, (6). Moreover, in 2000, it was identified a novel zinc metalloprotease with considerable homology to ACE called ACE2 which can cleave Ang I and Ang II to form angiotensin-(1-7) [Ang-(1-7)] and angiotensin-(1-9) [Ang-(1-9)], respectively (9) with also their receptors MAS-R and AT2-R, respectively (10,11) (**Fig. 2)**
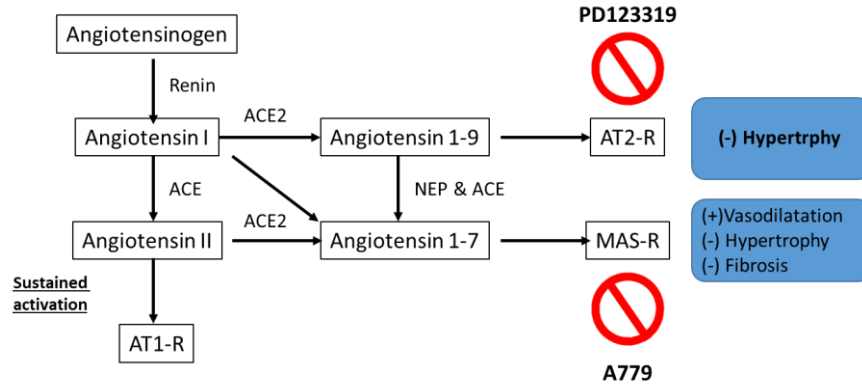
Fig. 2. Expanded view of the renin-angiotensin system, including the angiotensin-converting enzyme 2, to form angiotensin-(1-9) and angiotensin- (1-7), with their receptors and known physiological activity. PD123319, AT2-R antagonist and A779, MAS-R antagonist. Adapted from Fyhrquist et al. Renin-angiotensin system revisited. J Intern Med. 2008; 264:224–34.

1.1.3. Dysregulation of the cardiovascular system

Cardiac hypertrophy. The heart must continuously pump blood to supply the whole body with oxygen and nutrients. To maintain the high energy consumption required by this role, the heart is equipped with different biological systems that allow its adaptation to changes in systemic demand. ANS and RAS have been extensively studied as neurohumoral mechanisms, initially activated upon stress to increase contractility and survival in the early phase, but which could become pathological in the chronic period (12). The hypertrophic growth of cardiomyocytes is the primary response by which the heart reduces the stress on the left ventricular wall imposed by pressure overload. It entails stimulation of intracellular signaling cascades that activates gene expression and promotes protein synthesis, protein stability or both, and organization of force-generating units (sarcomeres), which, in turn, lead to increase size of individual cardiomyocytes (13). However, an enlargement of the heart in response to chronic hypertensive stress, myocardial injury, or excessive neurohumoral activation is associated with cardiac dysfunction and is described as "pathological hypertrophy" (14). Pathological hypertrophy associates with increased cardiomyocytes death and fibrotic remodeling, and it is characterized by a reduced systolic and diastolic function that often progresses towards heart failure. Primary triggering events of cardiac hypertrophy such as mechanical stress and

neurohumoral stimulation contribute for the modulation of various cellular responses including gene expression, protein synthesis, sarcomere assembly and cell metabolism, leading to the development and progression of cardiac hypertrophy (15,16)

1.2.   Cardiomyocytes

Cardiomyocytes are terminally differentiated cells performing the contractile work in the heart. These cells have lost their ability to generate cardiac growth during hypertrophy results primarily from an increase in cellular protein content, with little or no change in cardiomyocyte number (17). In the early embryonic stage, the cardiomyocyte precursor seems to be much more dependent on glycolysis as a source of energy, and mitochondrial oxidative metabolism is poorly developed. However, the successful transition of embryonic stem cells to cardiomyocytes requires a switch from glycolytic metabolism to mitochondrial oxidative phosphorylation to meet increases in energy demand (18).

1.2.1.   Special organelle requirements

Mitochondria. This organelle occupy approximately 30% of the total volume on the cardiomyocytes and produce around 6 kg of ATP/day through oxidative phosphorylation, to sustain cardiac mechanical function (19), In addition to ATP production, mitochondria regulate cell death and survival by integrating a range of cellular signals; they are also the primary source of reactive oxygen species (ROS), which can trigger oxidative stress, thereby affecting cell survival and death (20)

Endoplasmic reticulum (ER). The ER, among its several essential functions, the most remarkable on the cardiomyocytes is being a dynamic calcium reservoir, which can be activated by both electrical and chemical stimulation (21). It contains the IP3 receptor (IP3R) and ryanodine receptor (RyR), responsible for releasing Ca^{2+} in response to the input signals (22), counteracted by sarco/endoplasmic reticulum

Ca^{2+}-ATPase (SERCA), that functions to maintain the internal store of Ca^{2+} at the expense of ATP hydrolysis (23)

1.2.2. Function

Cardiomyocyte contraction. The contraction of the heart is regulated by changes on intracellular calcium, where an action potential is sensed by the cardiomyocytes, causing the entry of Ca^{2+} to the cells via L type calcium channels (LTCC) located in T tubules, establishing an inward Ca^{2+} current that, in turn, triggers massive Ca^{2+} release from the sarcoplasmic reticulum (SR) via RyR2 in a process called "calcium-induced, calcium release (CICR)". The rise in intracellular Ca^{2+} induces chemo-mechanical coupling in which Ca-binding to cardiac troponin C (cTnC) triggers a series of protein-protein interactions releasing the thin filaments from inhibition and promoting force-generating cooperation between myosin cross-bridges and actin. The rise in intracellular Ca^{2+} is transient as highly effective processes actively transport the Ca^{2+} back into cellular storage depots within the sarcoplasmic reticulum or back to the extracellular space through the inhibitory phospholamban protein (PLN) or by Na^+/Ca^{2+} exchanger (NCX) respectively (24) permitting the relaxation.

1.3. Cardiomyocyte hypertrophy

1.3.1. Calcium and hypertrophy.

Beyond its role in triggering contraction/relaxation and contributing to the electrical stability of the cardiomyocyte, intracellular Ca^{2+} ($[Ca^{2+}]i$) is also critically involved in cell signaling and on some pathological onsets. One of the most studied calcium signaling pathways is the Ca^{2+} dependent calcineurin-NFAT, which is principally related in mediating pathological cardiac hypertrophy and inflammation (25). Mediators from the neurohumoral systems such as catecholamines (e.g., norepinephrine) and Ang II, bind to seven-transmembrane receptors that are coupled to G proteins. Gq signaling, activates phospholipase C (PLC), catalyzing the

synthesis of inositol 1,4,5 triphosphate (IP3), which induces intracellular Ca^{2+}-release activating the calcineurin/NFAT signaling (25). The phosphatase protein calcineurin dephosphorylates NFAT in the cytoplasm, inducing its nuclear translocation with the subsequent expression of genes involved in hypertrophy. Activation of calcineurin/NFAT signaling alone is sufficient to induce pathological cardiac hypertrophy (26). Ca^{2+}-dependent signaling is also involved in cardiomyocyte stress-responses and apoptosis, which additionally contribute to the impaired myocardial function. Indeed, reduced SR Ca^{2+} content, as is known to occur in failing cardiomyocytes, has been linked to activation of the unfolded protein response, apoptosis, and altered SR structure (27). Finally, disrupted Ca^{2+} homeostasis is known to offset the finely tuned balance between energy demand and availability in the heart. Energy wasting during heart failure results from futile Ca^{2+} cycling, and ATP production is reduced following Ca^{2+}-mediated mitochondrial dysfunction (28).

1.3.2. RAS and cardiomyocyte hypertrophy.

At a cellular level, the main effector of the RAS system Ang II binds to specific seven-transmembrane receptors coupled to heterotrimeric proteins of the Gαq/α11 subclass. These proteins are coupled to phospholipase Cβ (PCβ). This coupling induces the generation of diacylglycerol (DAG), which functions as an intracellular ligand for protein kinase C (PKC) leading to PKC activation, and production IP3 (29), which leads to the mobilization of internal Ca^{2+} by directly binding to the IP3R located in the ER or the nuclear envelope. The release of Ca^{2+} to the intracellular space has shown to mediate hypertrophic signaling through activation of calcineurin-NFAT or calmodulin-dependent kinase (CaMK)-HDAC inactivation. Activation of Gαq/α11 is also a potent inducer of MAPK signaling in cardiac myocytes, although the exact mechanism of MAPK coupling has not been described (30,31)

1.3.3. ANS and cardiomyocyte hypertrophy

Physiological sympathetic stimulation of the heart induced by epinephrine or norepinephrine (NE), increases its developed contractions (inotropy) and accelerate its relaxation (lusitropy) through β-adrenergic receptors, activating GTP-binding protein Gs, which stimulates adenylate cyclase to produce cAMP, which in turn, activates protein kinase A (PKA). This kinase phosphorylates several proteins related to excitation-contraction coupling (Phospholamban, LTCC, RyR, troponin I, and myosin-binding protein C (32). The lusitropic effect of PKA is mediated by phosphorylation of phospholamban and Troponin I, which speed up SR Ca^{2+} reuptake and dissociation of Ca^{2+} from myofilaments, respectively (33). The inotropic effect of PKA activation is mediated by the combination of increased ICa, greater availability of SR $Ca^{2+,}$ and the modulation of the open probability of RyR channels (34). NE, phenylephrine, or endothelin-1 also activates Gq/PLC/IP3 signaling inducing the growth of neonatal rat cardiomyocytes, along with an elevated expression of fetal genes (reprograming gene expression) such as those encoding atrial natriuretic peptide (ANP), brain natriuretic peptide (BNP), myosin light chain-2, or α and β-myosin heavy chain. Forced expression of CaMKII results in the same phenotypic changes as induction of neurohumoral agonist/Gq signaling, while pharmacological inhibition of CaMKII suppresses such adverse remodeling (35–37). CaMKII induces cardiomyocyte growth via phosphorylation of class II histone deacetylases (HDACs), especially HDAC4 and HDAC5, by promoting the export of these molecules from the nucleus, leading to depression of MEF-2-mediated gene expression and cardiac hypertrophy (38). In short, activation of CaMKII is sufficient to induce pathological cardiac hypertrophy.

1.3.4. Mitochondrial dynamics and cardiomyocyte hypertrophy.

Given the high density of mitochondria in cardiomyocytes and the absolute dependence on mitochondrial oxidative phosphorylation to generate ATP for cardiac contraction, it is not surprising that pathological alterations in this tissue are often associated with changes in mitochondrial metabolism or function. Changes in

mitochondrial metabolism, resulting in a general deterioration of the cardiac metabolic function, have been reported in advanced pathological hypertrophy (39). Although mitochondria are often depicted as isolated organelles, they are highly dynamic networks whose structure and distribution have a potential effect on metabolic function. The mitochondrial morphology depends then on balance between the opposing processes of mitochondrial fission and fusion (40). In mammalian cells, the primary regulators of mitochondrial fusion are dynamin-related GTPases termed mitofusins (MFN1 and MFN2) and optic atrophy protein 1 (OPA1). Conversely, mitochondrial fission protein 1 (FIS1) and the dynamin-related protein 1 (DRP1) are involved in mitochondrial fission (41). During the last years, several investigators have linked mitochondrial dynamics processes with cardiac hypertrophy or dysfunction. In 2008, Yu et al. (42) proved that mitochondrial fission mediated high glucose cell death through elevated production of ROS. In 2014, our group (43) showed for the first time that mitochondrial fission is required for cardiomyocyte hypertrophy via Ca^{2+}/calcineurin signaling pathway. In 2015, Wang et al. (44) showed that a microRNA regulating mitochondrial fission where associated with doxorubicin cardiotoxicity.

1.3.5. Cardiac gene expression and hypertrophy.

Reprogramming of cardiac gene expression consisting of upregulation and downregulation of particular sets of genes is critical in modulating heart function and has a fundamental role in the pathogenesis of cardiac hypertrophy and heart failure (45). In previous sections, we discussed the effect of specific transcriptional factors, activating or changing the transcription of certain proteins on the setting of cardiac remodeling or dysfunction. Nevertheless, another way to modify the expression of a particular gene into a protein or a set of proteins is through the epigenetic modifications or by the recently discovered non-coding RNAs:

Epigenetic modifications. Some of the latest advances in the study of gene expression regulation have been in the field of epigenomic change which comprises secondary chemical alterations of DNA (methylation of cytosines) and the proteins

around which the DNA is wound (post-translational modification of histones) which induce changes to the state of chromatin. Transcription is modulated by rendering the regulatory elements of genes permissive to the activity of transcription factors (46)

DNA methylation. This process is a highly conserved mark that signals for transcriptional repression. The methylation of DNA at position 5 of cytosine is performed by DNA methyltransferases (DNMTs) (47). DNA methylation regulates gene expression either by directly blocking transcription-factor binding or recruiting methyl binding proteins (MBD), which in turn interact with co-repressor complexes (48). Methylated DNA from cardiac biopsies is altered in patients with end-stage cardiomyopathy, and this differed significantly at the CpGs of promoters and gene bodies compared with healthy hearts. Increased gene expression in failing hearts was associated with promoter demethylation, whereas hypermethylation did not clearly correlate with decreased expression. Failing hearts were significantly hypomethylated at satellite regions, and this correlated with a 27-fold increase of the corresponding transcripts. In summary, these preliminary findings support a role for DNA methylation in dysregulation of gene expression associated with heart failure, but whether this epigenetic mark contributes substantially to pathogenesis remains uncertain, as do the underlying mechanisms of this process (49).

Histone modifications. Histone can undergo acetylation on lysine residues, promoting relaxation of chromatin structure and, therefore, transcriptional activation or methylation on lysine and arginine residues, with either activation or repression of transcription depending on the degree (monomethylation, dimethylation or trimethylation) and the location of the modification. Histone acetylation is a highly dynamic modification and is regulated by the opposing action of two families of enzymes: Histone acetyltransferases and histone deacetylases (HDACs) (50). Histone acetyltransferases use acetyl coenzyme A as a cofactor to catalyze acetylation and are divided into two major classes. Type A is nuclear and includes N-acetyltransferase 6 (NAT6), the MYST family (named after the founding members

MOZ, Ybf2, Sas2, and TIP60), and CBP/p300 proteins. By contrast, type B is predominantly cytoplasmic. Several reports have indicated the importance of p300 in cardiac development and heart failure through transcription controlled by myocyte-specific enhancer factor (MEF) 2 and transcription factor GATA-4 (51). Eleven HDAC members have been identified, and they are subdivided into four classes (I–IV) according to cellular localization, enzymatic activity, and protein structure. The role of HDACs in cardiac hypertrophy and failure is complex: some HDACs have anti-hypertrophic actions, whereas others promote hypertrophy (52).

As with histone acetylation, histone methylation is a dynamic process regulated by two classes of enzymes: histone methyltransferases and histone demethylases. Methylation at H3K4, H4K36, or H3K79 is associated with transcriptional activation, and methylation at H3K4 and H3K36 is implicated in mRNA elongation. Conversely, methylation at H3K9, H3K27, or H3K20 is linked with transcriptional repression. Several reports have suggested that histone methylation is involved in cardiac hypertrophy and failure; for example, lysine-specific demethylase 4A has shown to promote cardiac hypertrophy under pathological conditions (53). Upregulation of the hypertrophy markers atrial and B-type natriuretic peptide in a mouse model and patients with heart failure was not caused by altered acetylation of their promoters, but rather by decreased dimethylation and trimethylation of lysine 9 on histone H3 (54). H3K79-specific histone-lysine N-methyltranferase has shown to be critically involved in defining the transcriptional landscape of differentiating cardiomyocytes. Of note, expression of this histone methyltransferase was found to be downregulated in patients with idiopathic dilated cardiomyopathy, and its cardiac-specific disruption in mice resulted in dysregulation of dystrophin and the development of a dilated-cardiomyopathy like phenotype (55).

Non-coding RNAs. A large part of the genome is transcribed, but not translated into protein. 'Canonical' (protein-coding) genes account for only ~1.5% of the genome, whereas >80% is transcribed into ncRNA. ncRNAs are divided into two classes based on size: small ncRNA (<200 nucleotides long) include microRNA (miRNA), piwi-interacting RNA (piRNA), and endogenous short- interfering RNA (siRNA); by

contrast, long non coding RNAs (lncRNA) form a highly diverse class, united essentially by a length of >200 nucleotides and a general lack of protein-coding capacity. Specific ncRNAs have been linked to the control of many cellular functions, particularly in the development and pathological processes (56).

microRNAs (miRNAs). microRNAs (miRNAs) are endogenous small non-coding RNAs of 18-25 nt in length. miRNAs are transcribed mainly by RNA polymerase II as pri-miRNAs, which are usually several thousand bases in length. They are subsequently processed in the nucleus into a 70-100 nt hairpin RNAs (pre-miRNAs) by the RNase III-type enzyme drosha, and cleaved by Dicer in the cytoplasm to form the mature double-stranded miRNAs. This double-stranded mature RNA can then exert its function of post-transcriptional regulation of gene expression incorporating one strand to the miRNA-induced silencing complex (miRISC) to bind target mRNA through its seed sequence, binding of mature miRNAs to mRNAs usually results in the repression of target gene expression by either degrading the target mRNA or inhibiting the translation (62) Each miRNA could repress up to hundreds of transcripts, and it is thus hypothesized that miRNAs form large-scale regulatory networks across the transcriptome through miRNA response elements (MREs)

Several miRNAs have shown to be dysregulated in cardiac hypertrophy. In 2006, a group of investigators compared the microRNA expression of a transverse aortic constriction (TAC) model with a calcineurin transgenic mouse model, both showed a specific group of miRNAs similarly dysregulated, and they largely mimic the one of the idiopathic end-stage failing human heart (63). Other groups of investigators revealed after profiling studies that the expression of the dysregulated miRNAs progressively changed during the development of pressure-overload cardiac hypertrophy (64). Overexpression of specific fetal miRNAs in cultured cardiomyocytes triggers fetal gene expression and induces cellular hypertrophy, suggesting that altered miRNAs might have essential roles in initiating this process (65). It appears that miRNA dysregulation can affect multiple cellular processes in way that are conducive to the establishment of cardiac diseases.

Long non-coding RNAs (lncRNAs). These RNAs constitute a heterogeneous class of transcripts that they have been grouped solely based on their length by knowledge of the nucleotide sequence alone. The capacity of lncRNAs to fold into a variety of thermodynamically stable secondary structures such as double helices, hairpin loops, bulges, and pseudoknots allowing the formation of complex tertiary interactions that enable them to interact with the wide range of macromolecules, including other RNA species, DNA, and proteins to generate ribonucleoprotein particles (46). Based on the molecular mechanism. lncRNAs can be classified as signalers, protein decoys, guides, or scaffolds and are divided into nuclear and cytoplasmic types (57). The nuclear types can either downregulate transcription, by guiding chromatin modifiers to specific genomic loci to prompt a repressive heterochromatin state or activate transcription via recruitment of histone-lysine-N-methyltransferase 2A and by acting like enhancers (58). The cytoplasmic lncRNAs repress or stimulate gene expression at the transcriptional level by binding or sequestering miRNAs and preventing them from affecting translational repression (46). A restricted number of lncRNAs have been found to be highly regulated in cardiac hypertrophy. Nevertheless, they can act in concert with microRNAs to modulate cardiac hypertrophic growth. In 2014, a lncRNA was identified as cardiac hypertrophy related factor (CHRF) which induces hypertrophy in vitro and apoptosis in vivo by acting as a sponge for miR-489 (59). The same group also identified a cardiac-apoptosis-related lncRNA (CARL), that interacts with miR-539 like a sponge to inhibit mitochondrial fission (60). The lncRNA heavy-chain-associated RNA transcripts (MHRT), was recently shown to affect cardiac hypertrophy, remodeling, and progression to heart failure (61).

1.4. Angiotensin-(1-9)

1.4.1. State of the art.

The RAS is without question one of the most prominent endocrine, paracrine, and intracrine vasoactive systems in the physiological regulation of neural, cardiovascular, blood pressure, and kidney function. The importance of the RAS in the development and pathogenesis of cardiovascular, hypertensive and kidney diseases has been firmly established (7) and inhibiting or blocking the classical axis of this system, with its main effector, Ang II, is currently one of the most used therapies in cardiovascular diseases with outstanding results (66). However, the RAS has expanded from the classic axis to include several other complex biochemical and physiological axes. In the present study, we will focus on one of these recently described alternative axes and its main effector, the Ang-(1-9). This nine-amino acid peptide from the non-canonical RAS is produced by hydrolysis of the carboxy-terminal leucine from angiotensin I, through the catalysis of the ACE2 (67) or by the action of a serine peptidase from platelets named deamidase (9). ACE2 also produces Ang-(1-7) through hydrolysis of Ang II, thereby reducing available levels of it. It was initially thought that Ang-(1-9) functioned merely as an intermediate step in the pathway with no physiological effects.

In 2002, Jackman et al. (68) reported that Ang-(1-9) was able to increase arachidonic acid and nitric oxide (NO) in human pulmonary arterial endothelial cells and that this peptide was significantly more active than Ang-(1-7) in doing this. ACE2 catalyzes the cleavage of Ang I to Ang-(1-9) but ACE inhibitors do not inhibit it and its transcripts are found mainly in the heart, kidney, and testis of human tissues (67). Nevertheless, the protein expression of ACE2 was found reduced in the kidney of diabetic Sprague-Dawley rats (69), and the use of enalapril (ACE inhibitor) attenuates its downregulation in the late phase of ventricular dysfunction in the myocardial infarcted rat (70). Interestingly, the administration of Ang-(1-9) to myocardial infarcted rats by osmotic minipumps, decreased plasma Ang II levels, inhibited ACE, and also prevented cardiomyocyte hypertrophy via AT2R (71). In 2012, Flores et al. (72) showed that Ang-(1-9) reduces cardiac fibrosis, inhibits

fibroblast proliferation, and increases contraction via the AT2R in stroke-prone spontaneously hypertensive rats. They also suggested that Ang-(1-9) also improved basal NO bioavailability. To further investigate Ang-(1-9) effects and the counter-regulatory axis of the RAS, the same group of investigators engineered adenoviral vectors expressing fusion proteins that release Ang-(1-7) and Ang-(1-9) to assess the effects on hypertrophy in rat H9c2 cells or primary adult rabbit cardiomyocytes. Their results showed that both peptides inhibit cardiomyocyte hypertrophy via MasR and AT2R, respectively (72). Consecutively, Ang-(1-9) also reduces hypertension, ameliorates cardiac hypertrophy, fibrosis, and oxidative stress in the heart and the aorta and improved cardiac endothelial function in hypertensive rats (73). Additionally, Ang-(1-9) treatment attenuated cardiac hypertrophy, reduced cardiac fibrosis, and improved ventricular function in streptozotocin (STZ)-induced diabetic rats by reducing mRNA levels of TNF and IL (74). In 2016, Fattah *et al.* (75) also showed that gene therapy with Ang-(1-9) preserved systolic function after myocardial infarction, protected against hypertrophy and fibrosis and also proved for the first time a positive inotropic effect by increasing calcium transient amplitude on isolated cardiomyocytes and increased contraction in a Langendorff model through a PKA-dependent mechanism. Finally, our group depicts that Ang-(1-9) protected the myocardium against ischemia/reperfusion injury through an AT2R and Akt-dependent mechanism after performing experiments *in vitro*, *in vivo* and *ex vivo* in rats (76).

1.4.2. Our recent novel insights.

Our group showed that Ang-(1-9) stimulated the appearance of abundant interconnected mitochondria in the cardiomyocytes, mainly in the perinuclear region (Fig. 3A). Mitochondrial network integrity was assessed according to the number and volume of individual mitochondria through the 3D reconstitution of confocal stacks (43,77). Ang-(1-9) led to a gradual time-dependent decrease in the number of mitochondria per cell, to 75% (±9%), and 59% (±3%) of control levels after 3 and 6 h, respectively (Fig. 3B, left panel). Ang-(1-9) concomitantly increased mitochondrial volume by 72% and 158% after 3 and 6 h, respectively (Fig. 3B, right panel). To

investigate whether the changes in the mitochondrial network structure involves alterations in mitochondrial biogenesis or mitochondrial degradation, we evaluated mitochondrial mass by quantifying the abundance of the constitutive mitochondrial protein mtHsp70. Ang-(1-9) did not alter total mtHsp70 levels, suggesting that a change in mitochondrial turnover did not accompany the morphological changes (Fig. S1). Taken together, these data indicate that Ang-(1-9) either induce mitochondrial fusion or decrease mitochondrial fission in cardiomyocytes
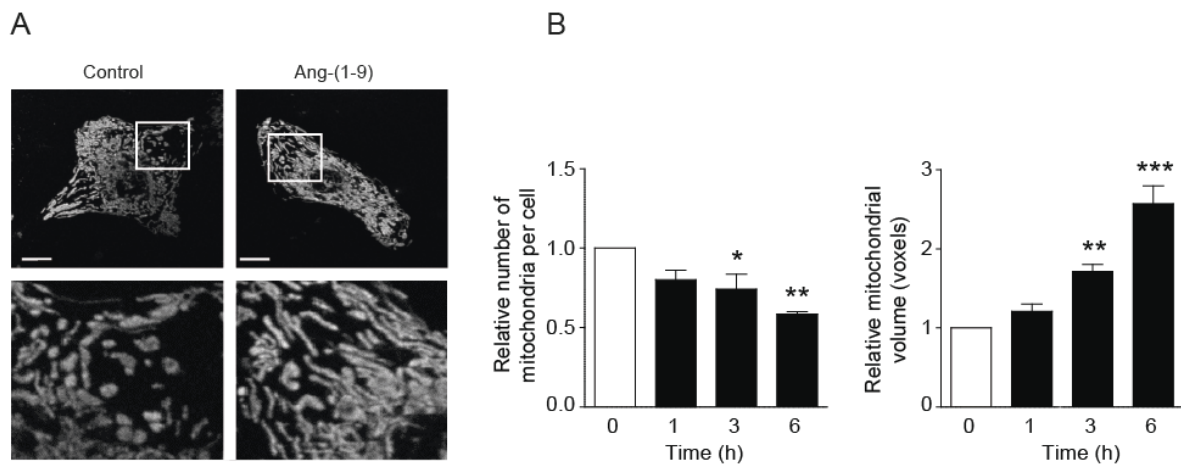
Fig. 3. Mitochondrial morphology of cardiomyocytes stimulated with 100 µM Ang-(1-9) for 0-6 h and then loaded with MitoTracker Green (MTG). Z-stack images were obtained with confocal microscopy (A). Scale bar: 2 µm. Lower panels represent a 15X magnification. (B) Quantification of the relative number of mitochondria per cell (left) and the relative mean mitochondrial volume (right) as mitochondrial dynamic parameters in cells treated with 100 µM Ang-(1-9) for the indicated times (n=4), $^{*}p<0.05$; $^{**}p<0.01$ and $^{***}p<0.001$ vs. 0 h.

Previous work established that the anti-hypertrophic effects of Ang-(1-9) are mediated by AT2R activation (10,73). Consistent with this evidence, the effects of Ang-(1-9) on mitochondrial morphology were entirely prevented by the AT2R antagonist PD123,319 (Fig. 4A-B), and not affected by the pharmacological MAS receptor antagonist A779 (Fig. 4C-D).
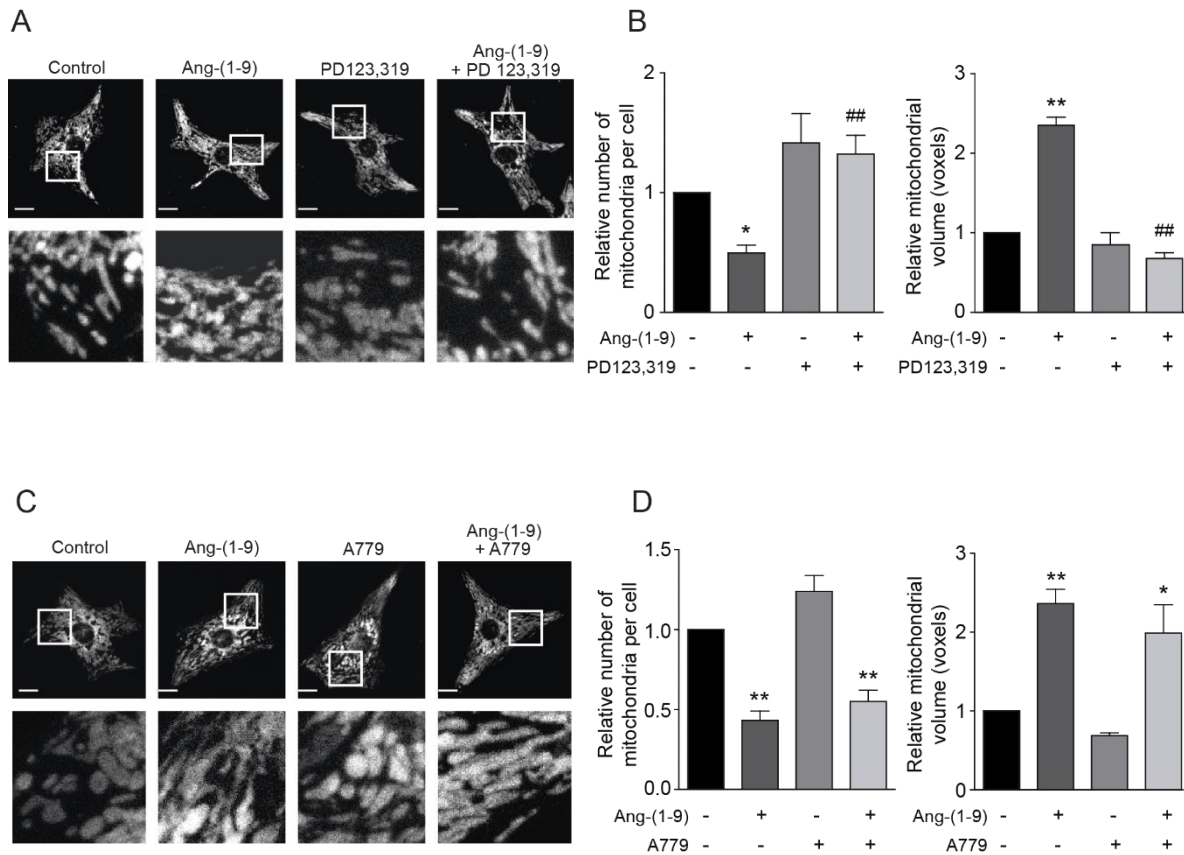
Fig. 4. Confocal microscopy images of cardiomyocytes treated with Ang-(1-9) (100 µM, 6 h) and AT2R antagonist (PD123,319; 1 µM) (A) or MasRr antagonist, (A779; 10 µM) (C) and then loaded with MitoTracker Green (MTG). Z-stack images were obtained with confocal microscopy. Scale bar: 2 µm. Lower panels represent a 15x magnification. (B, D) Mitochondrial number and mean mitochondrial volume for each condition were quantified (n=4 for B and n=3 for D). *$p<0.05$; **$p<0.01$ vs. control and ##$p<0.01$ vs. Ang-(1-9).

To study the molecular mechanisms by which Ang-(1-9) regulates mitochondrial dynamics, levels of mitochondrial fusion (Opa1 and Mfn2) and fission (Drp1 and Fis1) proteins were assessed by Western blot. Neither Opa1/Mfn2 nor Drp1/Fis1 protein levels were altered by Ang-(1-9) (Fig. S2). Because previous studies have established that Drp1 migration from the cytosol to Fis1-containing fission points on the mitochondrial surface is an initial step in mitochondrial fragmentation (43,78), we then evaluated whether Ang-(1-9)-triggered mitochondrial fusion was associated with changes in Drp1 distribution, especially moving away from the mitochondrial surface. Immunofluorescence studies showed that the punctate distribution pattern of Drp1 was disrupted by 6 h of Ang-(1-9) treatment (Fig. 5A). Moreover, Ang-(1-9)

36

decreased the effective colocalization of Drp1 with Fis1 (p<0.05), but not the effective colocalization of Fis1 with Drp1 (Fig. 5B), as indicated by the Manders' coefficient. This result suggests that Drp1 shows a reduced mitochondrial distribution after Ang-(1-9) stimulation, whereas Fis1 remains associated with the mitochondria under both conditions.
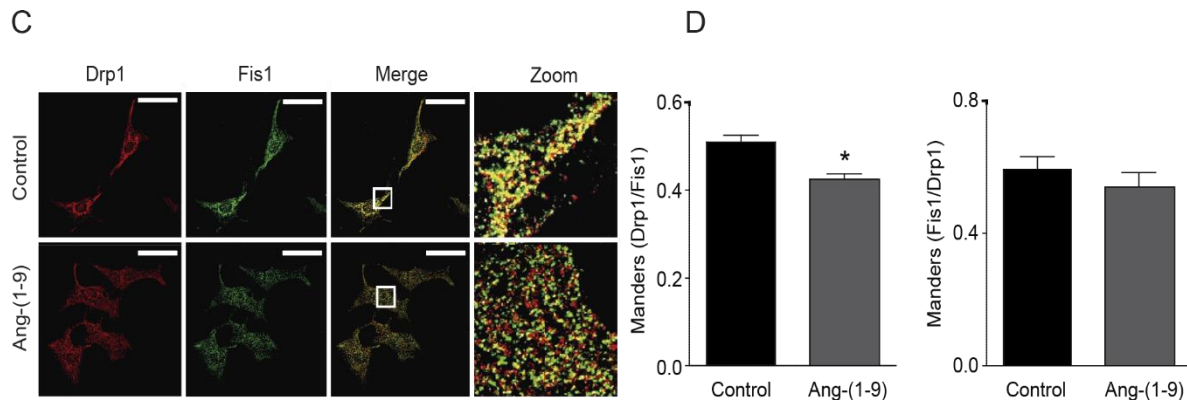
Fig. 5. Sub-cellular localization of the mitochondrial fission protein Drp1 visualized using immunofluorescence. Cardiomyocytes were stimulated with Ang-(1-9) for 6 h, incubated with anti-Drp1 and anti-Fis1 antibodies, and then visualized with confocal microscopy. Scale bar: 10 μm. Right panels represent a 45X magnification. The Manders' coefficients of the Drp1 and Fis1 signals were used as indicators of Drp1 localization in the mitochondria (n=3) *p<0.05 vs. control.

Pursuing this line of research, we assessed Drp1 phosphorylation status at Ser^{637}, a site that can inactivate the protein (79,80). Total Drp1 was immunoprecipitated and then probed with a Ser^{637}-specific antibody. As shown in Fig. 6A, Ang-(1-9) increased Drp1 phosphorylation to levels only slightly lower than those obtained using forskolin, a known inhibitor of the Drp1-fission pathway (81,82). Furthermore, Ang-(1-9) also decreased Drp1 phosphorylation on Ser^{616} (Fig.6B), a fission-promoting modification (83). In conclusion, these results strongly suggest that Ang-(1-9) decreases mitochondrial fission, rather than increasing mitochondrial fusion, to bring about the observed changes in cardiomyocyte mitochondrial morphology.

A

B
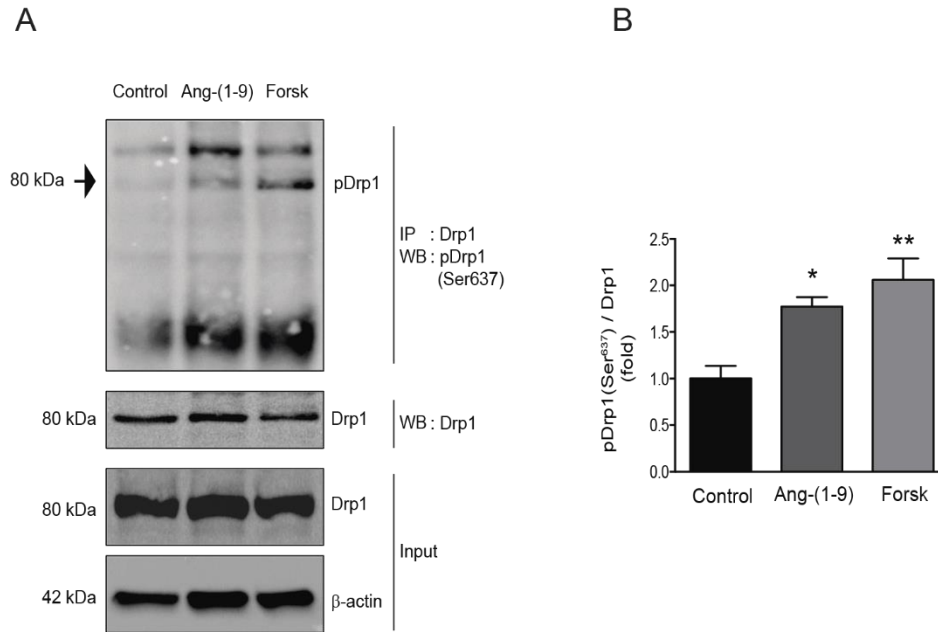
Fig. 6. Drp1 phosphorylation (pDrp1; Ser[637]) was assessed by Western blotting after immunoprecipitation of Drp1 protein. Cells were treated with Ang-(1-9) for 6 h or a pulse of 100 nM forskolin for 30 min (positive control for pDrp1). A representative image is shown for 3 independent experiments with similar outcomes. *$p<0.05$ and **$p<0.01$ vs. control

Finally, electronic microscopy was performed to compare the effects of Ang-(1-9), compared with NE and untreated cells over the mitochondrial morphology, as this is the gold standard for this type of analysis. Ang-(1-9) was sufficient to induce mitochondrial fusion and inhibit mitochondrial fission in NE-treated cardiomyocytes, corroborating the confocal microscopy studies (Fig. 7).
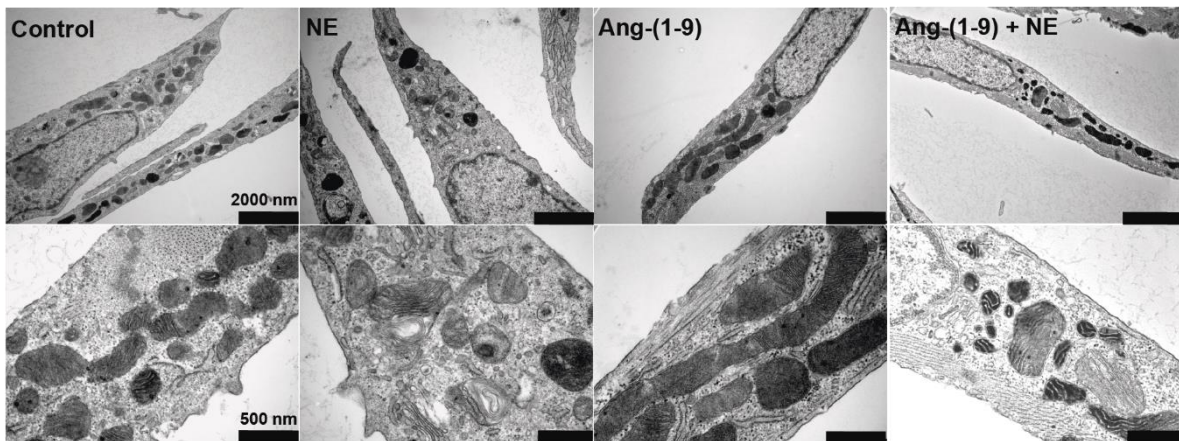
Fig. 7. Representative transmission electron microscopy images from Ang-(1-9)- and NE-treated cells showing two different magnifications of the same cells.

2.   GENERAL AIM

The present study aims to elucidate the differential miRNA expression induced by Ang-(1-9) and evaluate if this correlates with its known effects on calcium regulation and pathological cardiac growth prevention.

3.   SPECIFIC AIMS

- To investigate the microRNA expression patterns induced by angiotensin-(1-9) and norepinephrine in cardiomyocyte hypertrophy model

- To screen and evaluate the differentially expressed microRNAs induced by both treatments (in case there are any) against gene targets related to calcium signaling and/or cardiac hypertrophy using bioinformatic approaches

- To use biological or chemical inhibitors to evaluate if the blocking on changes in microRNA expression patterns induced by our treatments could also block or modulate the biological already known effects.

4. PRELIMINARY RESULTS

To begin this Ph.D. thesis, calcium measurements were made to study if the proven effects of Ang-(1-9) over the mitochondrial morphology were sufficient to affect somehow the handling of this ion and its signaling pathways, trying to establish a relationship or path between these effects and the ones described for the cardiomyocyte hypertrophy. After this, we aimed to prove some previous information regarding the effects of Ang-(1-9) over cardiomyocyte hypertrophy to establish the model to keep working on.

4.1. Neonatal cardiomyocytes as model of study.

Neonatal cardiomyocytes, while having lost mitotic activity, can be readily separated from one another. These cells lose their rectangular shape but maintain the ability to contract in culture when stimulated. These cells also undergo hypertrophy in response to several different agonists as well as mechanical stimuli, and these cells have been the primary source of information about intracellular signaling pathways involved in these cellular growth responses (84).

4.2. Ang-(1-9) regulates cytosolic Ca^{2+} levels.

Calcium measurments were performed to evaluate if the mitochondrial morphological changes induced by Ang-(1-9) could affect the calcium handling inside the cell. Considering that the treatment with this peptide can induce a more fused mitochondrial state together with the fact that a more connected mitochondrial network, with higher membrane potential, endows the mitochondria with greater Ca^{2+} buffering efficiency (85). Actually, it has been shown that inhibition of fusion or induction of fission weakens mitochondrial metabolic reserve, producing deregulated Ca^{2+} oscillations in skeletal muscle cells (86). Using a cytoplasmic Ca^{2+} dye, Fura-2, we monitored NE-triggered cytosolic Ca^{2+} levels (43) and found that this signal was reduced in cells pretreated with Ang-(1-9) ($p<0.05$ and <0.01 at 3 and 6 h, respectively) (Fig. 8A-B).
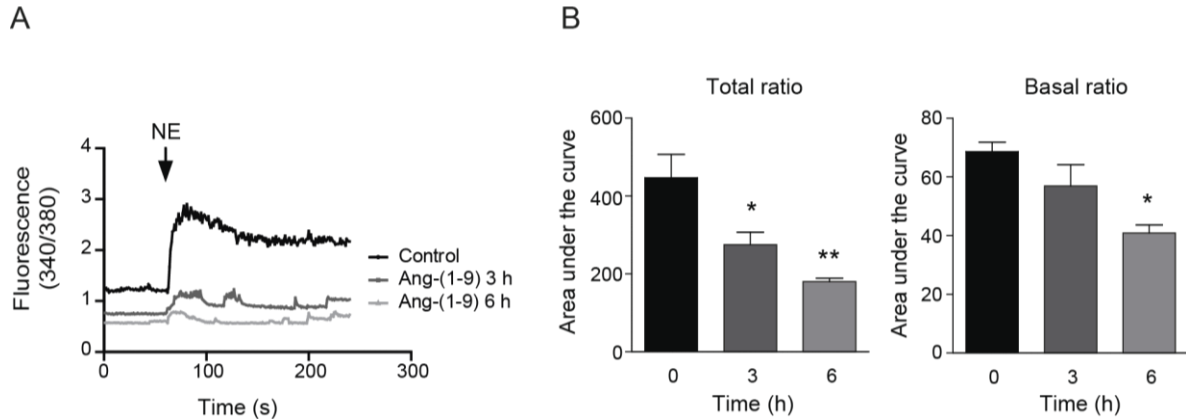
Fig. 8. Cytosolic calcium levels in cardiomyocytes treated with Ang-(1-9) and then challenged with NE. (A). Cells were loaded with Fura-2AM and then visualized in a confocal microscope. Fura-2AM fluorescence ratio (340 nm /380 nm) was quantified (B). A NE pulse (10 µM) was added to elicit an increase in cytosolic Ca^{2+}. Total (left) and basal (right) area under the curve were quantified (n=3). *$p < 0.05$ and **$p < 0.01$ vs. control.

To determine whether the lowering of cytoplasmic calcium was somehow explained by action over the mitochondrial calcium handling, Rhod-FF-preincubated cardiomyocytes were treated with histamine, which evokes an IP3-dependent release of Ca^{2+} (Fig. 9A) and changes in mitochondrial Ca^{2+} uptake were assessed. Interestingly, Histamine-stimulated mitochondrial Ca^{2+} uptake was significantly higher in cardiomyocytes pretreated with Ang-(1-9) ($p < 0.01$; 3 and 6 h) than in vehicle-treated control cells (Fig. 9B).
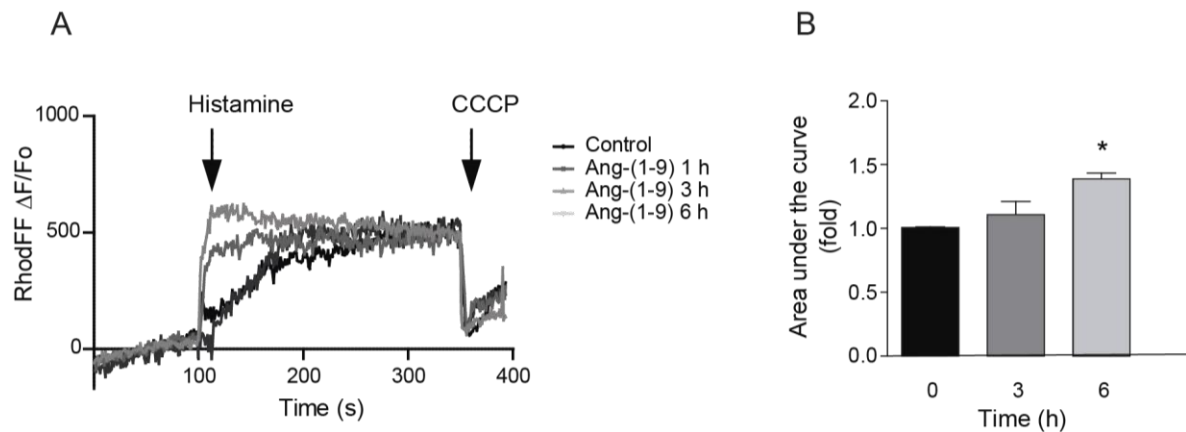
Fig. 9. Mitochondrial Ca^{2+} levels in cardiomyocytes treated with 100 µM Ang-(1-9) for 6 h and then loaded with Rhod-FF. Rhod-FF fluorescence kinetics were captured using confocal microscopy (A). A histamine pulse (100 µM) was added to elicit Ca^{2+} release from the endoplasmic reticulum, while CCCP (50 µM) was used to inhibit mitochondrial Ca^2 uptake. (B) The area under the curve of the Rhod-FF signal was determined from the curve (n=4).

Furthermore, and regarding the more prominent and more sustained effects of 6 h Ang-(1-9) treatments (cytoplasmic and mitochondrial calcium), this time was then used to evaluate against the well-known pro-hypertrophy agent norepinephrine Interestingly treating the cardiomyocytes with Ang-(1-9) prevented the less efficient mitochondrial Ca^{2+} uptake in cells under this model as seen in Fig.10A-B.
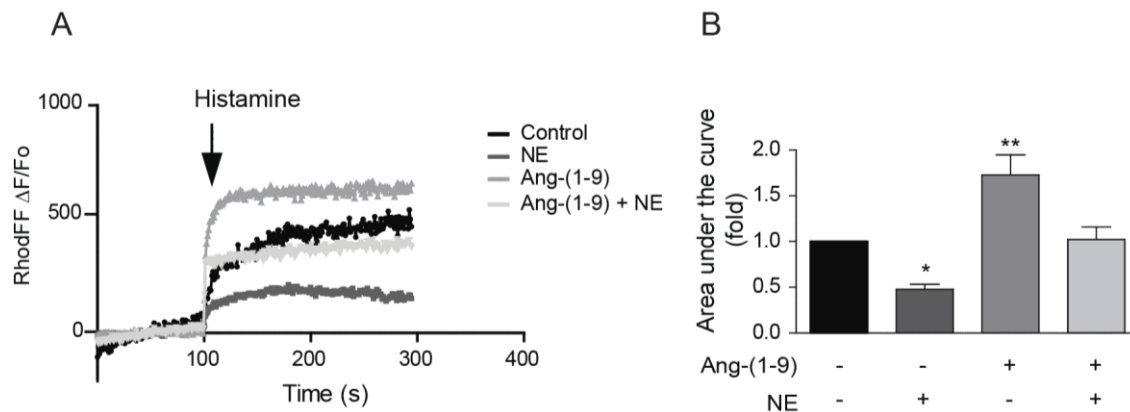
Fig. 10. Mitochondrial Ca^{2+} levels were measured in Rhod-FF-loaded cardiomyocytes. (A)Cells were pre-incubated with 100 µM Ang-(1-9) for 6 h and then stimulated for 24 h with NE. Rhod-FF fluorescence kinetics were visualized with confocal microscopy. A histamine pulse (100 mM) was added to trigger Ca^{2+} release from the ER. (B) The area under the curve of Rhod-FF signals are shown (n=3). *$p<0.05$ and **$p<0.01$ vs. control.

Neither Norepinephrine (NE) nor Ang-(1-9) induce rapid changes in mitochondrial calcium levels in the absence of histamine (Fig. S3), reinforcing the Ca^{2+} buffering theory. AT2-R antagonist blocked the effect of Ang-(1-9), and MAS-R antagonist showed no significant difference compared to control (Fig. S4)

4.3. Ang-(1-9) regulates ER-mitochondria contact sites.

Our group previously reported that NE-stimulated cardiomyocytes lose a significant number of ER-mitochondria contact sites, resulting in a functional decline in mitochondrial Ca^{2+} uptake capacity (87). Sites of physical contact between the ER and mitochondria are crucial for Ca^{2+} transfer between these organelles (88). To evaluate whether ER-mitochondria distance was altered in the Ang-(1-9)- and/or NE-treated cardiomyocytes, the colocalization of ER and mitochondria was measured using immunofluorescence and indirect labeling of specific proteins (87,89,90).

Fig.11A shows representative images of control and Ang-(1-9)- and/or NE-treated cardiomyocytes labeled with Fis1 (red) and KDEL (green) to detect mitochondria and ER, respectively. The colocalization of the two organelles was assessed in the whole cell by calculating the Manders' coefficient (89,91). The Manders' coefficient for Fis1/KDEL denotes the fraction of mitochondria that colocalizes with ER, whereas the Manders' coefficient for KDEL/Fis1 denotes the fraction of ER that colocalizes with mitochondria. Fis1/KDEL was significantly reduced in NE-treated cardiomyocytes as compared to controls, indicating movement of mitochondria away from sites of contact with the ER. This change was absent in the cells pretreated with Ang-(1-9) (Fig.11A-C).
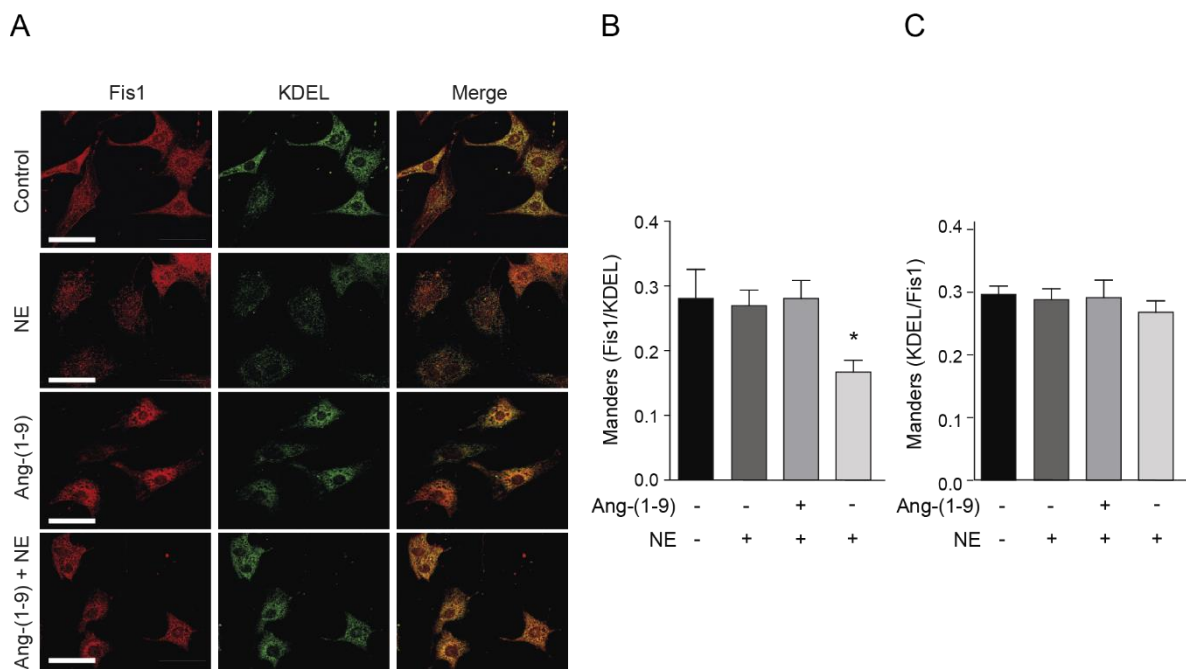
Fig. 11. Representative immunofluorescence images of cardiomyocytes stained with anti-FIS1 and anti-KDEL to visualize mitochondria and ER, respectively. (A) Cells were pre-incubated with 100 μM Ang-(1-9) for 6 h and then stimulated for 24 h with NE. Scale bar: 10 μm. (B) Manders' coefficients of FIS1- and KDEL-derived fluorescence were determined from the images obtained in (A) to quantify mitochondria and ER colocalization (n=3). *$p < 0.05$ vs. control.

4.4. Ang-(1-9) regulates cardiomyocyte hypertrophy and mitochondrial dynamics.

Confocal microscopy experiments were performed to prove that Ang-(1-9) prevented NE-induced hypertrophic growth in cardiomyocytes. As seen in Fig.12, double-staining revealed that NE-treated cardiomyocytes exhibited a hypertrophic phenotype, as indicated by the increased sarcomeric organization. Also, it is possible to visualize a larger cell perimeter and a decreased relative mitochondrial area as compared to controls (Fig. 12B). As expected, Ang-(1-9) prevented these NE-dependent changes in sarcomeric structure and abundance (Fig. 12) as well as relative cell size (Fig. 13). Ang-(1-9) also prevented the NE-dependent decrease in the mean size of individual mitochondria.
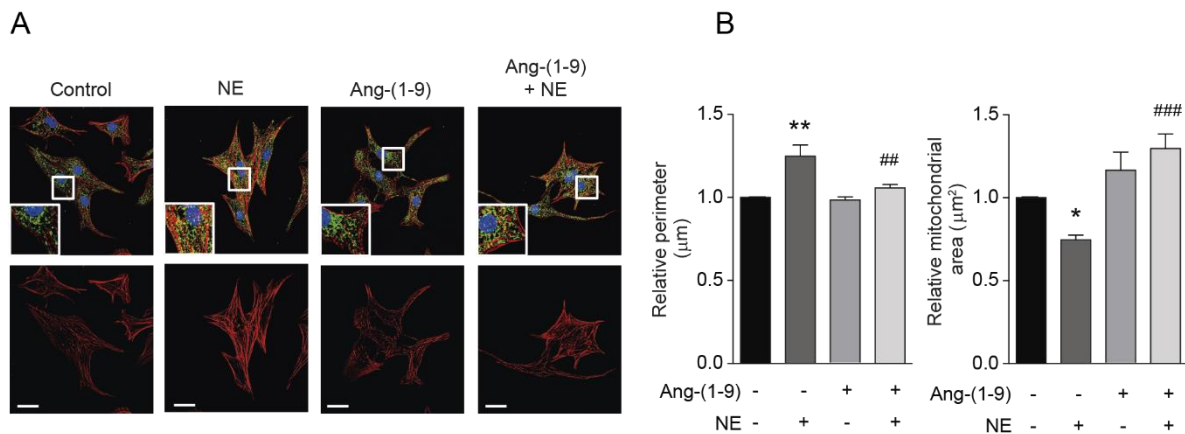
Fig. 12. A: Representative confocal images of cardiomyocytes treated with 100 μM Ang-(1-9) for 6 h and then stimulated with 10 μM of norepinephrine (NE) for 24 h. Cardiomyocytes were stained with rhodamine phalloidin to detect sarcomeric structures and immunolabeled for the mtHsp70 protein to identify the mitochondrial network. Scale bar: 25 μm. **B:** Quantitative analysis (n=4) of relative cellular perimeter and mitochondrial area of cardiomyocytes. $^*p<0.05$; $^{**}p<0.01$ and $^{***}p<0.001$ vs. control; $^{\#\#}p<0.01$ and $^{\#\#\#}p<0.001$ vs. NE.

4.5. Ang-(1-9) regulates Ca^{2+}/Calcineurin pathway.

Finally, the Ca^{2+}/calcineurin-dependent pathway was assessed in our model, considering that calcium is one of the main second messengers involved inthe signaling pathways induced by some pro-hypertrophic agents like NE with its molecular target, the nuclear factor of activated T cells (NFAT), mediating the

hypertrophic transcriptional response (43,92). Genes responsive to calcineurin/NFAT include the exon four isoform of the Rcan1 gene, which encodes an endogenous feedback inhibitor of calcineurin activity (43,80). An increase in Rcan1.4 expression or RCAN1.4 protein levels is often used as a molecular marker of calcineurin pathway activation. Interestingly, Ang-(1-9) blocked NE-induced activation of calcineurin signaling, as demonstrated by its effects on RCAN1.4 protein (Fig. 13A-B) and transcript levels (Fig. 13C). These findings are consistent with a model in which Ang-(1-9) stimulation prevents downstream activation of calcineurin by NE.
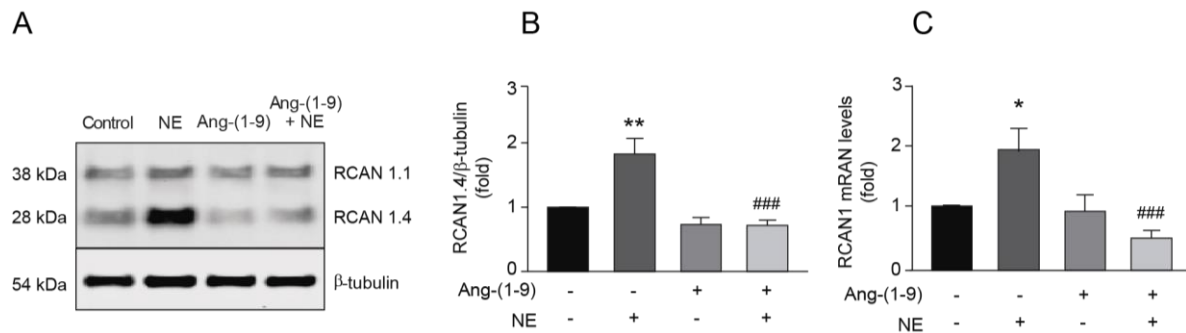
Fig. 13. Western blotting for RCAN1 isoforms in cardiomyocytes treated with angiotensin-(1-9) and NE. Cells were stimulated and then subjected to Western blotting using RCAN1 antibody. β-tubulin was used as a loading control. (F) Quantification of RCAN1.4 protein and (G) mRNA levels (n=4). *p<0.05 and **p<0.01 vs. control; ###p<0.001 vs. NE.

5. MATERIALS & METHODS

5.1. Bioethics.

All studies conformed with the Guide for the Care and Use of Laboratory Animals published by the US National Institutes of Health (NIH Publication, 8th Edition, 2011) and were approved by our Institutional Ethics Review Committee.

5.2. Reagents.

Antibodies against phospho- and total CREB were from Abcam. MitoTracker Green FM, Rhod-FF AM, Fluo3 AM, Fura-2, Alexa fluorescent secondary antibodies, FBS, and PKI [14-22]-myr were from Invitrogen. Anti-FIS1, anti-mtHsp70, and anti-KDEL antibodies were from ENZO Life Sciences. H89 was purchased from Calbiochem. Anti-β-tubulin and anti-β-actin antibodies, carbonyl cyanide m-chlorophenylhydrazone (CCCP), DMEM, M199 medium, norepinephrine, PD123319 ditrifluoroacetate, and other reagents were from Sigma-Aldrich Corp. A-779 was from Santa Cruz Biotechnology. Angiotensin-(1-9) was purchased from GL Biochem Ltd. All inorganic compounds, salts, and solvents were from Merck. Protein assay reagents were from Bio-Rad.

5.3. Cardiomyocyte culture.

Cardiomyocytes were isolated from the hearts of neonatal Sprague-Dawley rats, as described previously (43). Rats were bred at the University of Chile Animal Breeding Facility. Primary cell cultures were incubated with or without Ang-(1-9) (100 μM) and/or NE (10 μM) for 0–24 h in DMEM/M199 (4:1) medium, the presence or absence of the various inhibitors and other genetic reagents.

5.4. Cardiovascular hypertrophy assessment.

Sarcomerization was observed with confocal microscopy (Carl Zeiss LSM 5, Pascal 5 Axiovert 200 microscope) of methanol-permeabilized cells stained with rhodamine-phalloidin (1:400; F-actin staining) as previously described (43,93). For the cellular perimeter and mitochondrial area analysis, one focal plane of at least 50 cells from randomly selected fields was analyzed using ImageJ software (NIH).

5.5. Intracellular and mitochondrial calcium measurements.

Cytosolic Ca^{2+} levels were determined in cardiomyocytes preloaded with Fluo3-AM (5.4 µM, 30 min) or Fura2 (5 µM, 30 min), as described previously (94,95). To evaluate mitochondrial Ca^{2+} levels, images were obtained from cultured cardiomyocytes preloaded with Rhod-FF (5.4 µM, 30 min) (94–96). At the end of each measurement, 10 µM of CCCP was used as control (87) Both measurements were performed in an inverted confocal microscope (Carl Zeiss LSM 5, Pascal 5 Axiovert 200 microscope).

5.6. Western blotting.

Cell and tissue total protein extracts were analyzed as described previously (77,97). Protein contents were normalized to β-tubulin or β-actin.

5.7. RNA extraction.

Total RNA was isolated using TRIzol (Thermo Fisher Scientific) according to the manufacturer's instructions, including the addition of 20 µg of glycogen (Roche) prior to isopropyl precipitation. Every sample used for sequencing was measured its integrity and had a RIN (RNA integrity number) Above 9.0 (Fig. S5)

5.8. RT-qPCR.

Real-time PCR was performed with SYBR green (Applied Biosystems) as previously described (77). RCAN1.4 transcripts were normalized to 18S rRNA, whereas data for PKIA transcripts were normalized to mean β-actin and Hprt1 mRNA as internal control with the 2-ΔΔCt method. The qPCRs for each of the biological quadruplicates were performed in triplicate. Primers used were as follows:

RCAN1.4 rat forward 5'-CCCGTGAAAAAGCAGAATGC-3';
RCAN 1.4 rat reverse 5'-TCCTTGTCATATGTTCTGAAGAGGG-3';
PKIA rat forward 5'-CTACCATCAGAGACTGCCCC-3';
PKIA rat reverse 5'-TTGCTGTTGCCACTTGCAGA-3'.

5.9. Small RNA-seq cloning (TrueSeq System).

Total RNA (3 µg) with an RNA integrity number above 9.5 was ligated to a 3' adenylated adapter with a truncated RNA-ligase (New England Biolabs) and to a 5' adenylated adapter with T4 RNA-ligase (#M0204S, New England Biolabs) as previously described (98). cDNA synthesis was performed using a PCR amplification and SuperScript III first-strand cDNA Super Mix for 50 min at 50°C, and then 5 min at 85°C. 10 µL of the cDNA obtained in the previous steps was amplified using with index sequences and specific-Illumina sequences (desired TruSeq Index-primer, different for each sample), with a PCR program as described: 1 min at 98°C, 12 cycles (10 sec at 98°C, 10 sec at 60°C, 30 sec at 72°C), 10 min at 72°C and ∞ 4°C. We used 6% PAA SequaGel electrophoresis to select the successfully cloned and amplified sRNAs and ethidium bromide staining to visualize the results. The appropriate bands (ca. 140 bp) were cut out shredded, and eluted, and then filtered and precipitated. The resulting dscDNA quality and concentration was measured in each sample. Finally, each pellet was dissolved in water. Pool libraries were normalized and stored at -80°C, and deep sequencing was run on the HiSeq 1000 platform (Illumina). The quality of the library pool was assessed using a bioanalyzer (Agilent Technologies) (Fig.S6)

5.10. Small RNA differential expression analysis.

Raw reads were trimmed with the clipping of the first ten bases in each side using Trimmomatic version 0.36 (99) if average quality fell below the threshold of Q<30. A five-base sliding-window quality filtering was also performed, eliminating reads where the quality average of a window fell below Q<30. To reconstruct small RNA transcripts, transcripts were annotated, and expression levels estimated using a similar approach to that described by Orell et al. and Matamala et al. (100,101). Reads shorter than 15 nt after trimming were discarded, and the resulting clean data were mapped to the rat genome Rnor_6.0 (102) using Bowtie version 1.0.0 (103), allowing one mismatch and suppressing reads with more than ten alignments. SAM files generated on the mapping process were converted into BED format and used for coordinate-based assembly with BEDTools (104). Reads belonging to each assembled small RNA transcript were recovered and used to estimate expression levels. Transcriptional fragments with less than 50 reads in total were eliminated from the analysis. The functional annotation of each small RNA class was recovered based on genomic coordinate overlap using microRNAs from miRBase version 21 (105) and the ncRNAs from Ensembl version 92 (106) as a reference, retaining transcripts with an overlap of at least 50%. The final expression matrix generated from the assembly was used for differential expression analysis with DESeq2 version 1.28.0 (107). Transcripts were considered to show significant differential expression for p-value ≤0.05.

5.11. Conservation analysis between rat, mouse and human miRs.

Mature/primary sequences of mouse and human microRNAs were recovered from miRBase and mapped against the rat genome using Bowtie version 1.0.0 (103). Genomic coordinates of the mapped miRNAs were then cross-referenced with the small RNA transcripts generated in our RNA-seq assay, retaining regions with an overlap of at least 50%.

5.12. Northern blotting.

Northern blotting was performed as previously described (108). Briefly, 10 µg of total RNA was separated in a 12% SequaGel at 350 V for approximately 1 h. The gel was then stained with ethidium bromide and transferred at 20V for 30 min in a semi-dry chamber to an Amersham Hybond-N membrane (GE Healthcare), where the RNA was cross-linked to the membrane at 50ºC using an EDC-solution (Pall & Hamilton, 2008). Next, the membrane was incubated overnight at 50°C with a hybridization solution containing the miR-129-3p antisense sequence (ATGCTTTTTGGGGTAAGGGCTT) labeled with ^{32}P-ATP. After incubation, the membrane was washed, exposed, scanned, and analyzed with ImageQuant software (Quantity One 4.6.6).

5.13. miRNA target prediction.

Two different software tools were used to assess gene target prediction. Using different approaches and algorithms, both tools retrieved predicted regulatory targets for our microRNAs. The first, TargetScan 7.2 uses an improved method to predict targeting efficacy (109,110). The second, miRWalk 2.0, reports miRNA-binding sites within the complete sequence of a gene. It also combines this information with a comparison of binding sites resulting from 12 existing miRNA-target prediction programs to build a novel comparative platform of binding sites for the promoter, cds, and 5'- and 3'-UTR regions (111).

5.14. Transient miRNA transfection.

Cells were transfected either with anti-miR negative control #1 (Ambion, AM17010; 100 nM), anti-miR-129-3p (Ambion, AM10076; 100 nM), or pre-miR-129-3p (Ambion, PM10076; 50 nM), 24 h before the end of the experiment, using OptiMEM and Lipofectamine RNAiMAX, according to the manufacturer's specifications. The

final effects of anti-miR negative control (anti-miR-Control), anti-miR-129-3p and pre-miR-129-3p on miR-129-3p levels in cardiomyocytes are summarized in Supplementary Table 1.

Supplementary Table 1. Ct values of transfected cells

	n=1		n=2		n=3	
	miR-129-3p	**RNU6b**	**miR-129-3p**	**RNU6b**	**miR-129-3p**	**RNU6b**
Non-transfected	35.29	19.77	36.13	20.71	32.19	20.60
Anti-miR-Control	35.10	20.80	35.06	19.85	30.35	19.81
Anti-miR-129-3p	ND	19.80	ND	20.71	ND	19.69
Pre-miR-129-3p	19.8	19.71	21.29	21.27	17.49	19.69

5.15. Statistical analysis.

Data shown are mean ± SEM of the number of independent experiments indicated (n) and represent experiments performed on at least three separate occasions with similar outcomes. Data were analyzed by one-way or two-way ANOVA accordingly, and comparisons between groups were performed using a protected Tukey's test. Statistical significance was defined as $p < 0.05$.

6. RESULTS

6.1. RNA-seq studies

Taking together the fact that Ang-(1-9) treatment in our model were able to prevent calcium deregulation, loss of ER-mitochondria contacts and cardiomyocyte hypertrophy itself induced by NE, also proving that the calcineurin-NFAT signaling pathway was affected, not only at the protein expression level but also at the transcripts levels (Fig. 13), the main objective of this thesis was to further evaluate the complex underlying mechanism behind the protective effects of this peptide.

First, looking through the literature from other groups studying the RAS or the calcium dysregulations involved in the cardiac physiopathology, we found interesting data showing that many gene products contribute to cellular calcium homeostasis and that changes in their expression levels by a range of different microRNAs were tightly linked to cardiac dysfunction (112). In addition, these potent regulators of gene expression mediate the cardioprotective effect of ACE inhibition in acute kidney injury (113), and their dysregulation has a crucial role in cardiac fibrosis and hypertension induced by Ang II (114). Finally, because a complete microRNA expression profile produced either by Ang-(1-9) or by NE was never done before, we started our project by running RNA-seq studies on cultured neonatal rat cardiomyocytes treated for 6 h with Ang-(1-9), for 24 h with NE and 6 h and then 24 h consecutively (Ang-(1-9)/NE). We then evaluate the microRNA expression pattern induced by these treatments, compared with non-treated cells. RNA was isolated, purified, and subjected to small RNA expression profile analysis using an RNA-seq approach.

6.2. Bioinformatics analysis

The RNA-seq data for the three conditions (NE, Ang-(1-9), and Ang-(1-9)/NE) identified a total of 2,536 transcripts (Fig. 14), each of which was later compared with the small RNA classes reported in GFF format in the NCBI database as well as miRNAs recovered from miRBase for the Rnor_6.0 genome assembly (105). The analysis showed that 20% (499) of those transcripts shared annotation with known sRNA classes. We identified 345 transcripts (69% of annotated features) as miRNAs (Fig. 14), which were later used to perform a differential expression analysis using DESeq (107).
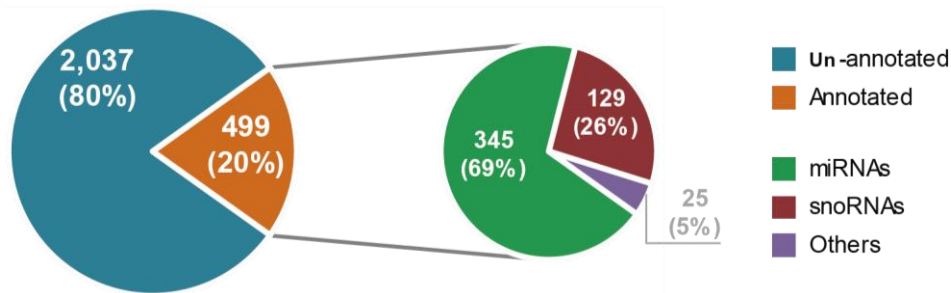
Fig. 14. miRNA identification from the RNA-seq data of cardiomyocytes treated with NE, Ang-(1-9)/NE, and Ang-(1-9) versus control. Each transcript was compared with the small RNA classes reported in the GFF format in the NCBI database, and the miRNAs recovered from miRBase for the Rnor_6.0 genome assembly.

We found 4, 11, and 21 miRNAs that were differentially expressed after NE, combined NE/Ang-(1-9) and Ang-(1-9) alone treatment, respectively (Fig. 15). Some miRNAs were differentially expressed in more than one condition; a total of 32 miRNAs showed distinct expression patterns compared to the control condition. Only two of these 32 miRNAs were differentially up-regulated, one after NE and the other after Ang-(1-9) treatment (Fig. 15).
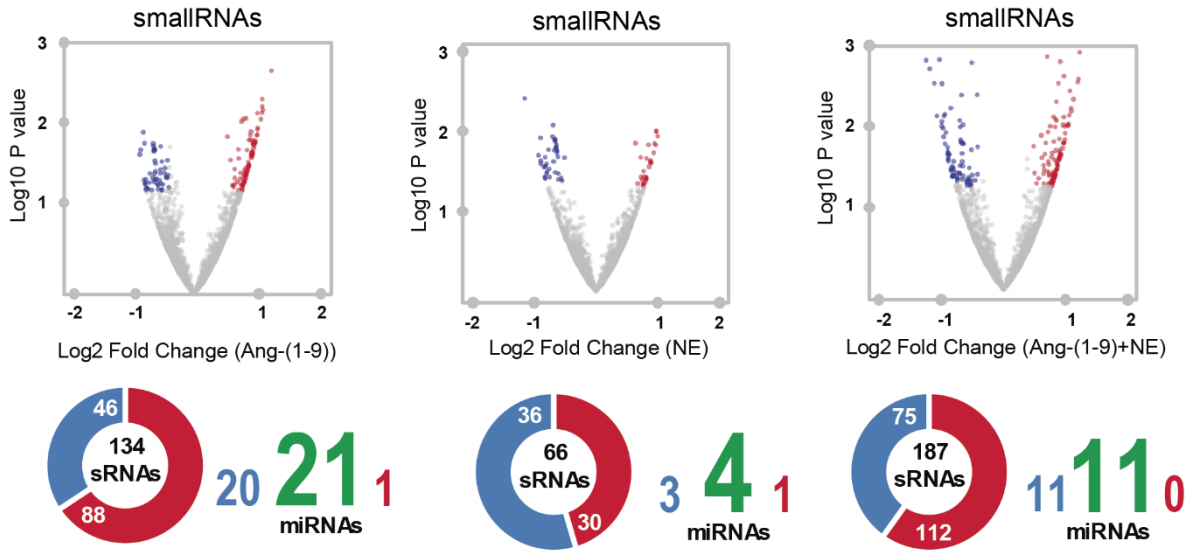
Fig. 15. Differential expression analysis using DESeq2. NE treatment triggered the differential expression of 4 miRNAs, whereas Ang-(1-9)/NE and Ang-(1-9) increased expression of 11 and 21 miRNAs, respectively.

Interestingly, a conservation analysis indicated that 24 of these differentially expressed neonatal rat cardiomyocyte miRNAs were present in both human and mouse, 6 were present in mouse but not human, and 2 were exclusive to the rat genome (Fig. 16).
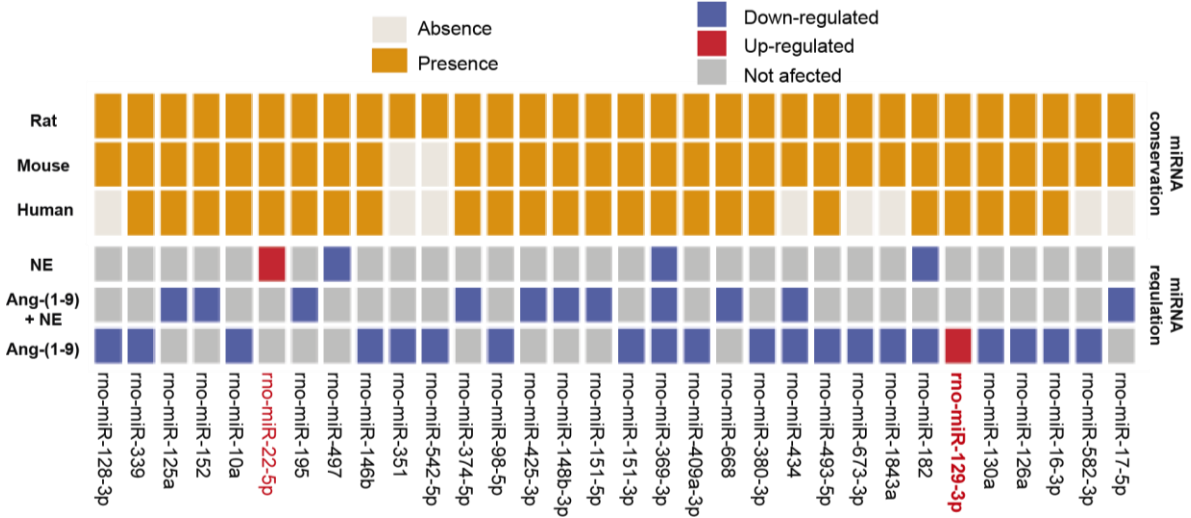
Fig. 16. Conservation analysis against human, mouse, and rat of the differentially expressed neonatal rat cardiomyocyte-miRNAs from the conditions in (B). 24 of these miRNAs were present in human and mouse, 6 in mouse, and 2 of them presented no conservation.

54

We selected the 24 conserved human/mouse miRNAs to generate a new filter, using the mean base values provided by DESeq2. Using a p-value ≤0.05 as the cutoff, the only up-regulated miRNA that was fully conserved among these mammals was miR-129-3p. Given the novelty of this finding in the context of cardiac hypertrophy, we evaluated this miRNA as a candidate for regulating the effects of Ang-(1-9) in cardiomyocytes (Fig. 17).
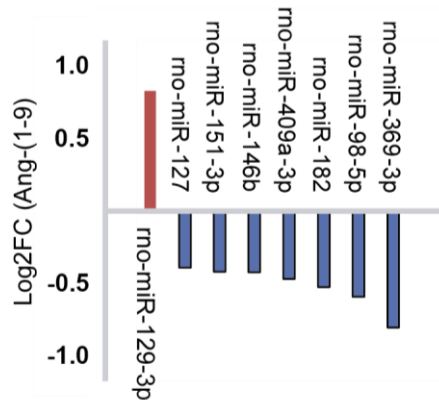
Fig. 17. Relative expression using the 24 differentially expressed miRNAs that were conserved in mouse, rat, and human, a new filter was generated using their base mean values provided by DESeq2. Finally, the highest LFC led us to focus on the only differentially up-regulated miRNA, miR-129-3p in the Ang-(1-9) treatment.

6.3. Candidate validation

Northern blotting was then performed to confirm the change in miR-129-3p expression following Ang-(1-9) treatment identified by our miRNA expression profiling (Fig. 17). Northern blotting is the gold standard to quantify miRNA levels for several reasons, but one of the most important ones is that there is no enzymatic manipulation of RNA. Other techniques such as qRT-PCR microarray require enzymatic manipulation that is sequence and structure-dependent and can introduce a non-linear bias between two different RNA populations (115). To get enough amounts of total RNA for the northern blotting, for this validation, we used Mef cell lines, which express the AT2R (116) and Hela cells as control (117).

Because the cell-cell contact could globally activate the microRNA biogenesis, leading to elevated mature miRNA levels and more forceful repression of target constructs (118) we first evaluate different conditions of confluence and serum deprivation to assess if our candidate miR-129-3p was affected by any of this conditions (Fig. 18).

Fig. 18. Northern blotting performed with 30 µg of total RNA extracted from Mef and Hela cell lines (lower images) and their corresponding ethidium bromide staining as RNA loading parameter. Conditions are: Pre-Conf (cells with 60% of confluence), Confluence (Cells with 100% confluence), Post-Conf-24 h (24 h after 100% confluence), Post-Conf-48 h (48 h after 100% confluence). Serum deprivation states for cells in media without serum.

After demonstrating that miR129-3p was not affected by confluence or serum deprivation conditions, we ran a time curve with Ang-(1-9), NE, and the AT2R antagonist PD.123319 (Fig. 19). As expected, the 6 h treatment with Ang-(1-9) showed the most significant change; meanwhile, the 24 h NE treatment not only did not up-regulate miR-129-3p but instead, it induced its downregulation.
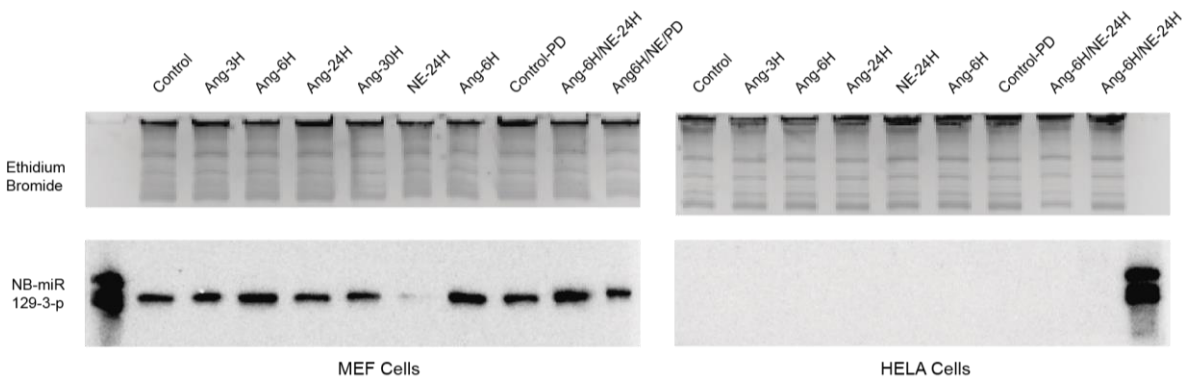
Fig. 19. Time curve northern blotting performed with 30 µg of total RNA extracted from Mef and Hela cell lines (lower images) and their corresponding ethidium bromide staining as RNA loading parameter. Conditions are: Ang-3H (3 h Ang-(1-9) treatment), Ang-6H (6 h Ang-(1-9) treatment), Ang-24H (24 h Ang-(1-9) treatment), Ang-30H (30 h Ang-(1-9) treatment), NE-24H (24 h NE treatment) and PD (AT2R antagonist).

Finally, we performed the experiment using the same conditions used for the RNA-seq.Adding the AT2R antagonist to investigate if the Ang-(1-9) effects over the miR-129-3p could be diminished or abolished when this receptor was blocked (Fig. 20)
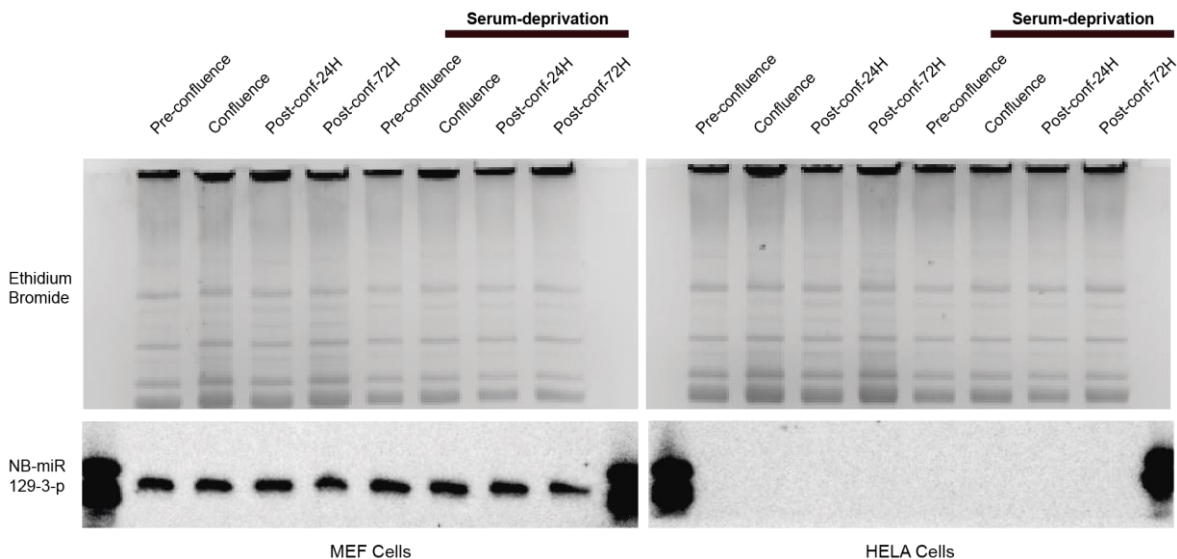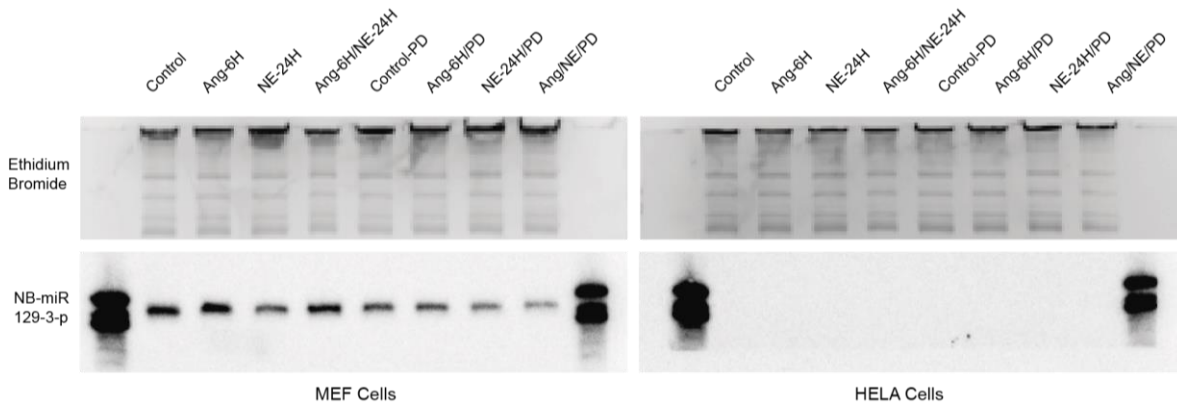

Fig. 20. Northern blotting performed with 30 μg of total RNA extracted from Mef and Hela cell lines (lower images) and their corresponding ethidium bromide staining as RNA loading parameter. Conditions are: Ang-(1-9) (6 h Ang-(1-9) treatment), NE-24H (24 h NE treatment) and PD (AT2R antagonist).

Finally, after stripping the membrane and probing it against RNU6 as a loading control, it was proved indisputably that Ang-(1-9) effectively was able to increase the levels of miR-129-3p (Fig. 21).
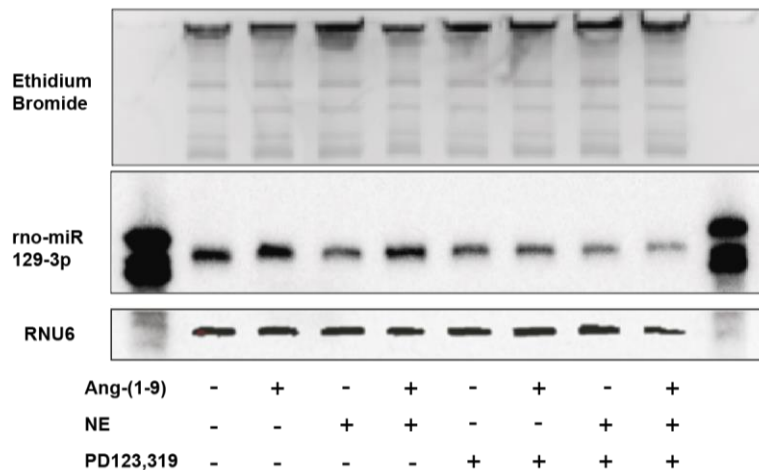
Fig. 21. Representative Northern blot gel for total RNA of MEFs cells used for rno-mir129-3p evaluation in B. (B) Qualitative evaluation of rno-mir129-3p levels in MEFs cell treated with Ang-(1-9) 100 μM for 6 h and pretreated with the AT2R antagonist PD123,319 (1 μM). RNU6 was used as a RNA loading control. A representative image is shown in 3 independent experiments with similar outcomes.

With the northern blotting experiments, the bioinformatics analyses were validated. Interestingly, the pretreatment of the AT2R antagonist PD123319 was sufficient to block miR-129-3p up-regulation induced by Ang-(1-9), suggesting that the whole effect should be due to the interaction of this peptide with its receptor.

6.4. Gene target assessment

In silico analysis of specific target genes for miR-129-3p, using two independent prediction tools, TargetScan (110) and miRWalk (119), identified the cAMP-dependent protein kinase inhibitor alpha (PKIA) as an essential target of miR-129-3p (Figs 22-23). This protein interacts with PKA and inhibits the activities of both C alpha and C beta catalytic subunits (120), which notably had already implicated in the regulation of mitochondrial dynamics through Drp1 phosphorylation (79,90). The target site prediction revealed a 7mer-m8 seed region for miR-129-3p in position 588-594 of the 3' untranslated region (3' UTR) of the PKIA mRNA (Fig. 23).

| Target gene	Gene name	3P-seq tags + 5	Cumulative weighted context++ score	Aggregate PCT	Panther protein class
MAPK3	Mitogen -activated protein kinase 3	271	-1.06	0.61	non-receptor serine/ threonine protein kinase
HRK	Harakiri, BCL2 interacting protein (contains only BH3 domain)	19	-0.95	0.7	
MYCL	V-myc avian myelocytomatosis viral oncogene lung carcinoma derived homolog	10	-0.76	0.43	Basic helix-loop-helix transcription factor nucleic acid binding
CACNG8	Calcium channel, voltage-dependent, gamma subunit 8	5	-0.62	0.57	voltage-gated calcium channel
NFATC2IP	nuclear factor of activated T-cells, cytoplasmic, calcineurin-dependent 2 interacting protein	754	-0.51	0.19	
RCAN2	regulator of calcineurin 2	32	-0.49	0.8	Signaling molecule
PKIA	**Protein kinase (cAMP-dependent, catalytic) inhibitor alpha**	**542**	**-0.49**	**0.81**	**Kinase inhibitor**

Fig. 22. Top ranking list of target genes obtained from TargetScan 7.2, filtered using http://pantherdb.org (reference proteome dataset), by biological process and biological regulation.

Rat PKIA ENST00000396418.2 3' UTR length: 7154

Site type	Context++ score	Context++ score percentile	Weighted context++ score	Conserved branch length	PCT
7mer-m8	-0.49	99	-0.49	8.502	0.81

Fig. 23. Schematic representation of the miR-129-3p and its seed region targeting the 3'UTR PKIA gene, displaying different prediction parameters in terms of conservation, mismatching, and predicted efficacy based on TargetScan 7.2.

6.5. Gene target validation

This prediction was functionally validated by qRT-PCR of the PKIA mRNA in cardiomyocytes treated with Ang-(1-9) and/or NE, which showed a decrease in PKIA mRNA after Ang-(1-9) plus NE administration (Fig.24)

Fig. 24. Quantification of PKIA mRNA levels using RT-qPCR (n=5), *$p<0.05$.

Consistently, Ang-(1-9) treatment of cardiomyocytes resulted in CREB phosphorylation, as a readout of PKA activation in these cells (Fig.25)
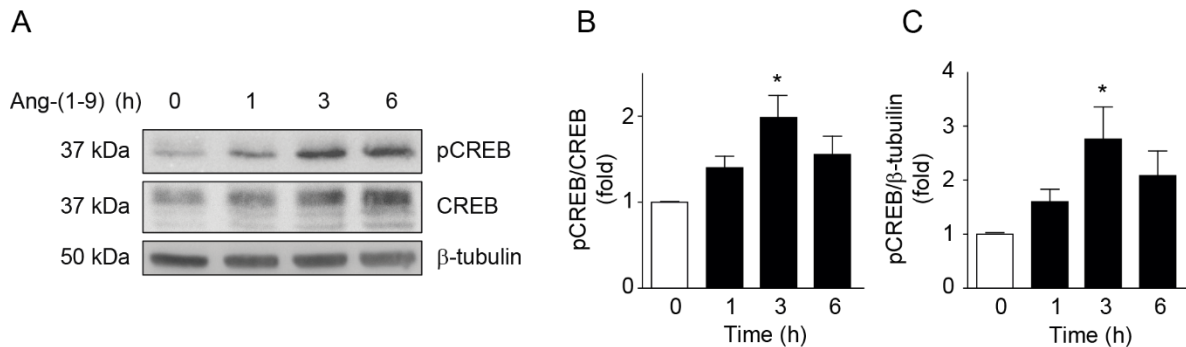
Fig. 25. pCREB, CREB, and β-tubulin levels were assessed by Western blotting of cells treated with 100 μM Ang-(1-9) for the indicated times (n=3) (A). Densitometric quantification of the Western blots (B, C). *$p < 0.05$ vs. 0 h.

6.6. Functional studies

To study the participation of the miR-129-3p/PKIA/PKA signaling pathway on Ang-(1-9) actions, we used several approaches. First, the pre-incubation of cardiomyocytes with H89, a chemical inhibitor of PKA, or a cell-permeable myristoylated form of PKIA. Secondly, the transient transfection of cardiomyocytes with antimiR-129-3p and the single transfection of cardiomyocytes with an artificial precursor of miR-129-3p.

6.7. PKA chemical inhibition

Using the PKA inhibitor H89, was sufficient to abrogate the anti-hipertrophic effect of Ang-1-9 in NE-treated cells. This data proved in some extent the need of PKA activation for Ang-(1-9) effects over cardiomyocyte hypetrophhy and mitochondrial morphology (Fig.26).
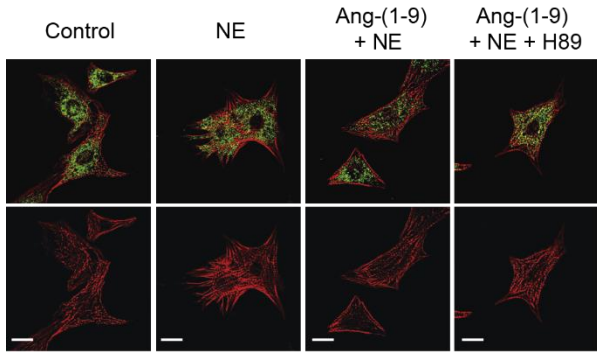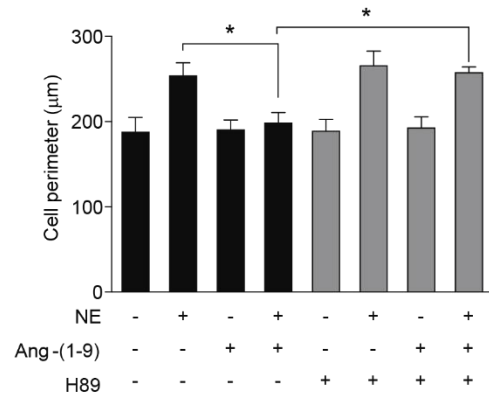
Fig. 26. Representative confocal images of cardiomyocytes treated with Ang-(1-9) 100 μM for 6 h and/or H89 10 μM and then stimulated with norepinephrine (NE) 10 μM for 24 h. The cells were stained with phalloidine rhodamine to detect sarcomeric structures and immunolabeled for the mtHsp70 protein to identify the mitochondrial network. Scale bar: 25 μm. (G) Quantitative analysis (n=3) of the cellular perimeter of cells in (F). *$p<0.05$; **$p<0.01$ and ***$p<0.001$ vs. control; #$p<0.05$; ##$p<0.01$ and ###$p<0.001$ vs. Ang-(1-9).

6.8. myrPKIA

To continue our validation, we tested a more selective end specific form of PKA inhibition using a myristoylated form of PKIA (the endogenous PKA inhibitor), trying to counterbalance the down-regulation of this peptide induced by Ang-(1-9). After performing the mitochondrial calcium measurements, using H89 and myr-PKIA, we were evidenced that both even blocked the normal increase of mitochondrial calcium triggered by histamine. This particular experiment leaded us to conclude that PKA blocking affects calcium handling *per se* and blocks completely the mitochondrial calcium uptake improvement induced by Ang-(1-9) (Fig.27).
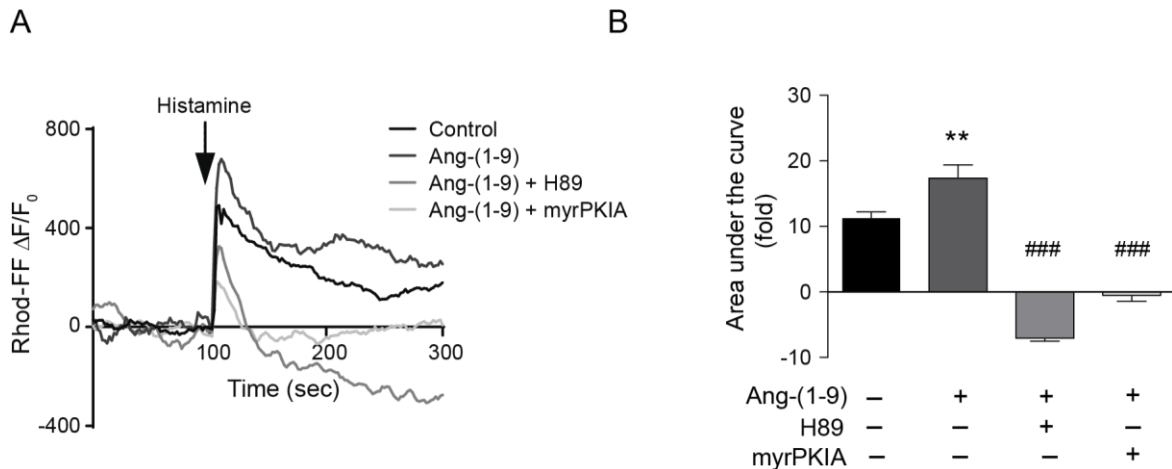
Fig. 27. Mitochondrial Ca^{2+} levels in cells stimulated with Ang-(1-9) after pre-treatment with the PKA inhibitors H89 (10 µM) or myrPKIA (10 µM) (A). Quantification of the area under the curve for Rhod-FF fluorescence (B) (n=3).

6.9. AntimiR/PremiR

Finally, to assess whether the effects of Ang-(1-9) were really through the up-regulation of miR-129-3p levels, we repeated the mitochondrial calcium experiment, but in this case, we transfected our Ang-(1-9)-treated cardiomyocytes with a Anti-miR-129-3p oligonucleotide. As seen in Fig.28, the use of AntimiR 129-3p, was sufficient to block the effects of Ang-(1-9) over mitochondrial calcium handling and on the other hand, the mere transfection of an oligonucleotide for increasing miR-129-3p levels (Pre-miR-129-3p), not only emulated the Ang-(1-9) effect over mitochondrial calcium handling, but also even improved it. Taken all this together, it´s possible to conclude that Ang-(1-9) exert its effects through the up-regulation of miR-129-3p and this affects directly the PKA activation and calcium handling inside of the cardiomyocytes.
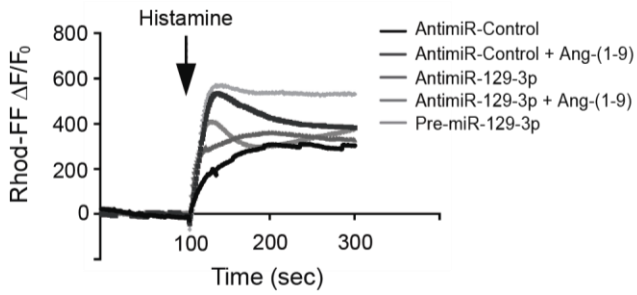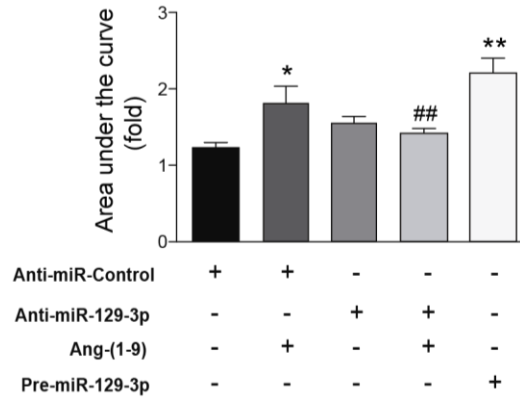
Fig. 28. Mitochondrial Ca^{2+} levels in cells stimulated as in A. (B) Quantification of the area under de curve for Rhodd-FF fluorescence (n=3) *p<0.05, **p<0.01 and ##p<0.05 vs Anti-miR-Control/Ang-(1-9).

6.10. Final model

Ang-(1-9) through its interaction with AT2-R up-regulates miR-129-3p, which on the one hand activates PKA, by blocking the effects of its natural endogenous inhibitor PKIA, and on the other hand, improves the mitochondrial calcium uptake, decreasing the total cytoplasmic calcium levels, preventing the activation of Ca^{2+}/Calcineurin/ NFAT signaling pathway, which could be one good explanation of the overall effects of this peptide over cardiomyocyte hypertrophy previously reported. In parallel to this, the PKA activation could be the reason for the effects ot Ang-(1-9) over mitochondrial morphology, which in turn, might explain the "better" capacity ot the mitochondria to uptake calcium.
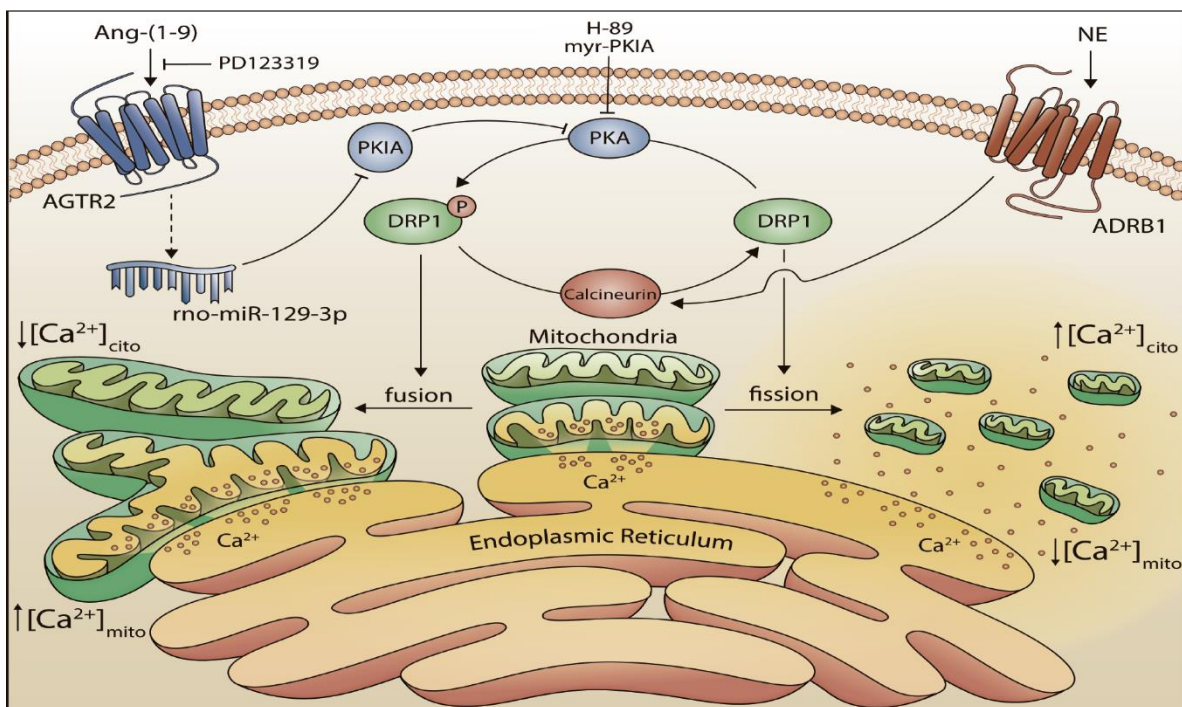
Final Model: Via miR-129-3p and PKA activation, Ang-(1-9) induces a more fused mitochondrial network through Drp1 phosphorylation and prevents NE-induced fission. These changes are associated with diminished cytoplasmic Ca^{2+} levels, increased ER-mitochondrial Ca^{2+} transport efficiency, and prevention of ER-mitochondria coupling loss.

7.   DISCUSSION

Ang-(1-9) is a non-canonical RAS peptide with anti-hypertrophic effects both *in vitro* and *in vivo*. These effects are mediated through AT2R activation (10,72,73); however, the downstream signaling pathways and intracellular effects of this peptide remain unknown. Preliminary information for this project showed that Ang-(1-9) was able to induce mitochondrial fusion and prevent mitochondrial fusion triggered by NE by unknown mechanisms (Fig. 3,7).

Here we show for the first time that Ang-(1-9) regulates Ca^{2+} handling in cultured rat cardiomyocytes, via up-regulation of miR-129-3p and inhibition of PKIA. Both alterations in mitochondrial dynamics and Ca^{2+} handling have been associated with the onset and progression of pathological cardiac hypertrophy (20). These changes are related to diminished cytoplasmic Ca^{2+} levels. Here, we showed that Ang-(1-9) prevents NE increases of $[Ca^{2+}]i$ and, consequently, NE-triggered calcineurin pathway activation.

7.1.   Calcium handling.

It has been previously reported that NE increases cytoplasmic Ca^{2+} levels, activating calcineurin, and thereby promoting calcineurin-mediated dephosphorylation of Drp1 to increase mitochondrial fission (43). In the absence of calcineurin activation, Drp1 would remain phosphorylated at Ser^{637} and the mitochondrial network intact. Ang-(1-9) decreased both baseline and NE-stimulated cytoplasmic Ca^{2+} levels, increasing ER-mitochondrial Ca^{2+} transport efficiency with the preservation of ER-mitochondria communication. The effects over intracellular calcium, furthermore, prevented the NE-dependent calcineurin activation as indicated by changes in *Rcan1.4*. mRNA and protein levels (Fig. 13). Mitochondria function as buffers for Ca^{2+}, particularly Ca^{2+} released from the ER. The efficiency of Ca^{2+} transfer from the ER to mitochondria is inversely dependent on the distance between these organelles

(121). NE causes a loss of ER-mitochondria contact sites, decreasing the efficiency of Ca^{2+} transport between these organelles (87). Ang-(1-9) treatment maintained Ca^{2+} transfer efficiency and prevented the loss of ER-mitochondria contact sites (Fig 11). Maintenance of ER-mitochondrial communication could indeed underlie the observed blunting of the cytoplasmic Ca^{2+} response induced by NE. However, Ang-(1-9) treatment did not increase the extent of ER-mitochondria contact at baseline. Therefore, physical changes in ER/mitochondrial coupling cannot explain the increase in Ca^{2+} transfer efficiency observed in the Ang-(1-9)-treated cells at baseline (Fig. 9). Another possible explanation for this change is the increased mitochondrial fusion found in the Ang-(1-9)-treated cardiomyocytes (Fig. 7). Mitochondria that are elongated or have a higher membrane potential show more efficient Ca^{2+} uptake (85).

The work of Fattah et al. suggests another potential mechanism for the observed increase in ER-mitochondrial Ca^{2+} transfer. These authors reported positive inotropic effects of Ang-(1-9) in isolated cardiomyocytes attributable to increased ER Ca^{2+} stores, likely through a PKA-dependent mechanism (75). Indeed, their findings agree with our results, and high ER Ca^{2+} stores may well contribute to the enhanced interorganellar Ca^{2+} transfer documented here. However, increased ER stores alone would not be sufficient to explain the suppression of cytoplasmic Ca^{2+} in response to NE. We propose that remodeling of the mitochondrial network toward a more fused state represents a vital aspect of the ability of Ang-(1-9) to buffer ER Ca^{2+} release and underlies its anti-hypertrophic effects. It is relevant to note that Drp1 Ser[637] can be phosphorylated by PKA, thereby acting in opposition to calcineurin to promote fusion. Thus, Drp1 phosphorylation may be an essential target of action for PKA in response to Ang-(1-9), in addition to the increased ER Ca^{2+} stores documented by Fattah et al. Notably, our miRNAs expression pattern studies indicated that miR-129-3p was the only miRNA up-regulated after Ang-(1-9) treatment. This miRNA, which has been implicated in angiotensin II signaling in HEK293 cells (122), would, in this case act downstream of the AT2R involved in the

inhibition of PKIA translation. Decreased PKIA signaling would directly impact PKA activation, potentially inducing Drp1 phosphorylation and increasing ER Ca^{2+} stores. Further studies are required to determine the relative contributions and possible interdependence of these two potential mechanisms of action.

The anti-hypertrophic effects of Ang-(1-9) are mediated by AT2R activation (10,72,73). Signaling through the G-protein coupled receptor is not well understood, although it is generally thought of as $G_{i\alpha}$ coupled. Therefore, the mechanism through which it might couple to PKA activity is not immediately apparent. Thus, understanding the signaling mechanisms of Ang-(1-9) immediately downstream of AT2R is an important contribution of this work. To our knowledge, this is the first report that associates miR129-3p with AT2R activation in cardiomyocytes, although this miRNA was previously described to be elevated in HEK293 cells after Ang II treatment (122). Notably, in this same work, treating cardiomyocytes with a biased angiotensin II analog significantly down-regulated miR-129-3p (122), which is consistent with the known pro-hypertrophic effects exerted by Ang II in cardiomyocytes and correlates with our results with Ang-(1-9) and its anti-hypertrophic properties.

Taken together, our studies show that Ang-(1-9) acts through AT2R to regulate mitochondrial morphology and Ca^{2+} uptake capacity via the AT2R/miR-129-3p/PKA signaling pathway. These effects are mediated by suppression of Drp1-dependent mitochondrial fission, increase mitochondrial Ca^{2+} buffering capacity, and preservation of ER-mitochondria contact sites following NE exposure. To our knowledge, this is the first study that links the Ang-(1-9)/AT2R/miR-129-3p/PKA signaling axis with control over mitochondrial dynamics.

7.2. PKA activation.

In the present work, we proposed activation of PKA protein by decreasing the levels of its endogenous inhibitor PKIA. In its inactive state, PKA exists as a tetramer of two regulatory (R) and two catalytic (C) subunits. Upon binding of two molecules of cAMP to each R subunit, the C subunits are released from the holoenzyme. These free C subunits can phosphorylate substrate proteins at Ser or Thr residues within the consensus sequence Arg-Arg- X-(Ser or Thr), where X denotes any neutral amino acid (123). These phosphoproteins regulate such diverse cellular functions as metabolism, ion transport, and gene transcription (124). Furthermore, the PKIA protein inhibits phosphorylation by the Cα and Cβ isoforms of the C subunit of PKA with equal efficiency and inhibits transcriptional activation by both isoforms. Because in many tissues, the C subunit pool is a mixture of Cα and Cβ, the ability of PKIA to inhibit both isoforms allows for negative regulation of all known PKA activity within the cell (120). In this context, here we showed that, together with previous work from our group, the PKA activation (not by cAMP) along with the lowering in cytoplasmic calcium (by the Improved entrance to mitochondria) are the key facts for the antihypertrophic effects of Ang-(1-9). It is noteworthy that norepinephrine (NE) also activates PKA but with a transient increase of intracellular calcium to improve contraction, activating calcineurin-NFAT signaling pathway and inducing, in a sustained activation, mitochondrial fission, and hypertrophic genes expression (5,26,82,125). In summary, the proposal of this work is that Ang-(1-9) exerts its effects through the activation of PKA (to some extent) without activating the Ca^{2+}/calcineurin/NFAT signaling pathway, unlike NE. The truthfulness of this asseveration would need more studies to evaluate, for instance, the exact extent of PKA induction by miR-129-3p in a more quantitative way compared to the PKA activation induced by different sources of cAMP.

Finally, the RNA-seq studies performed here also open the question of whether other members of the canonical and noncanonical RAS family could act through similar mechanisms. Given the newly-identified roles of the non-canonical RAS peptides Ang-(1-7) and Ang-(1-9) as counter-regulators of the ACE/Ang II axis and their recently-described ability to regulate blood pressure as well as cardiovascular and renal remodeling, our findings reveal an new important aspect of their modes of action, thereby providing novel approaches for therapeutic manipulation of these peptides and their biological actions in the cardiovascular system.

8.   HIGHLIGHTS

- Ang-(1-9) increased mitochondrial calcium uptake and prevented, to some extent, the cytoplasmic calcium rise induced by norepinephrine, together with the Ca^{2+}/Calcineurin/NFAT signaling pathway activation. The whole effect was blocked with an AT2R antagonist (PD123319)

- Ang-(1-9) prevented the reduction in endoplasmic reticulum-mitochondrial coupling induced by norepinephrine in cardiomyocytes, preserving the communication between organelles.

- RNA-seq studies showed that Ang-(1-9) up-regulates miR-129-3p levels in cardiomyocytes. The up-regulation was validated through northern blotting, and the use of AT2R antagonist blocked the up-regulation.

- Gene Target *in silico* studies showed that PKIA (PKA endogenous inhibitor) is a transcript target for miR-129-3p. These analyseswere validated qPCR, showing that Ang-(1-9) significantly decrease the PKIA transcript levels.

- Ang-(1-9) treatments were sufficient to activate PKA signaling pathway in accordance with its ability to decrease PKIA transcript levels.

- Treatments with a myristolyated form of PKIA blocked the effects of Ang-(1-9) over mitochondrial calcium. The chemical inhibition of PKA also blocked the effect of Ang-(1-9) over cardiomyocyte hypertrophy.

- The use of antimiR-129 blocked the Ang-(1-9) effects over mitochondrial dynamics. The treatment with premiR-129 alone was sufficient to increase the mitochondrial calcium uptake, completely emulating Ang-(1-9).

9. REFERENCES

1. Labrosse MR. Cardiovascular Mechanics. 2018. 400 p.

2. Nag AC. Study of non-muscle cells of the adult mammalian heart : a fine structural analysis and distribution . Cytobios. 1980;28(109):41–61.

3. Estigoy CB, Pontén F, Odeberg J, Herbert B, Guilhaus M, Charleston M, et al. Intercalated discs : multiple proteins perform multiple functions in non-failing and failing human hearts. Biophys Rev. 2015;(2009):43–9.

4. Ravenscroft SM, Pointon A, Williams AW, Cross MJ, Sidaway JE. Cardiac Non-myocyte Cells Show Enhanced Pharmacological Function Suggestive of Contractile Maturity in Stem Cell Derived Cardiomyocyte Microtissues. Toxicol Sci. 2016;152(1):99–112.

5. Lymperopoulos A, Rengo G, Koch WJ. The Adrenergic Nervous System in Heart Failure: Pathophysiology and Therapy. Circ Res. 2014;113(6):739–53.

6. Passos-silva DG, Brandan E, Augusto R, Santos S. Angiotensins as therapeutic targets beyond heart disease. Trends Pharmacol Sci [Internet]. 2015;1–11. Available from: http://dx.doi.org/10.1016/j.tips.2015.03.001

7. Stock P, Liefeldt L, Paul M, Ganten D. Local Renin-Angiotensin Systems in Cardiovascular Tissues: Localization and Functional Role. Cardiology. 1995;86:2–8.

8. Fyhrquist F, Saijonmaa O. Renin-angiotensin system revisited. J Intern Med. 2008;264:224–34.

9. Tipnis SR, Hooper NM, Hyde R, Karran E, Christie G, Turner AJ. A Human Homolog of Angiotensin-converting Enzyme. J Biol Chem. 2000;275(43):33238–43.

10. Flores-Muñoz M, Smith NJ, Haggerty C, Milligan G, Nicklin SA. Angiotensin1-9 antagonises pro-hypertrophic signalling in cardiomyocytes via the angiotensin type 2 receptor. J Physiol. 2011;4:939–51.

11. Santos RAS, Simoes AC, Maric C, Silva DMR, Machado RP, Buhr I De, et al. Angiotensin-(1–7) is an endogenous ligand for the G protein-coupled receptor Mas. PNAS. 2003;100(14):8258–63.

12. Shimizu I, Minamino T. Physiological and pathological cardiac hypertrophy. J Mol Cell Cardiol. 2016;97:245–62.

13. González A, Ravassa S, López B, Moreno MU, Beaumont J, José GS, et al. Myocardial Remodeling in Hypertension. Toward a New View of Hypertensive Heart Disease. Hypertension. 2018;72:549–58.

14. Hill JA, Olson EN. Cardiac Plasticity. N Engl J Med. 2008;358:1370–80.

15. Maillet M, Berlo JH Van, Molkentin JD. Molecular basis of physiological heart growth : fundamental concepts and new players. Nat Rev Mol Cell Biol [Internet]. 2013;14(1):38–48. Available from: http://dx.doi.org/10.1038/nrm3495

16. Lyon RC, Zanella F, Omens JH, Sheikh F. Mechanotransduction in Cardiac Hypertrophy and Failure. Circ Res. 2016;116(8):1462–76.

17. Heineke J, Molkentin JD. Regulation of cardiac hypertrophy by intracellular signalling pathways. Mol Cell Biol. 2006;7(August).

18. Lopaschuk GD, Jaswal JS. Energy Metabolic Phenotype of the Cardiomyocyte During Development , Differentiation , and Postnatal Maturation. J Cardiovasc Pharmacol.

2010;56:130–40.

19. Hall AR, Burke N, Dongworth RK, Hausenloy DJ. Mitochondrial fusion and fission proteins : novel therapeutic targets for combating cardiovascular. Br J Pharmacol. 2014;171:1890–906.

20. Vásquez-Trincado C, García-Carvajal I, Pennanen C, Parra V, Hill JA, Rothermel BA, et al. Mitochondrial dynamics , mitophagy and cardiovascular disease. J Physiol. 2016;3:509–25.

21. Bootman MD, Petersen OH, Verkhratsky A. The endoplasmic reticulum is a focal point for co-ordination of cellular activity. Cell Calcium. 2002;32:231–4.

22. Patel S, Joseph SK, Thomas AP. Molecular properties of inositol 1 , 4 , 5- trisphosphate receptors. Cell Calcium. 1999;25:247–64.

23. Clapham DE. Calcium Signaling. Cell. 2007;131:1047–58.

24. Solaro RJ. Sarcomere Control Mechanisms and the Dynamics of the Cardiac Cycle. J Biomed Biotechnol. 2010;2010:1–8.

25. Molkentin JD, Lu J, Antos CL, Markham B, Richardson J, Robbins J, et al. A Calcineurin-Dependent Transcriptional Pathway for Cardiac Hypertrophy. Cell. 1998;93:215–28.

26. Houser SR, Molkentin JD. Does Contractile Ca 2 + Control and Pathological Hypertrophy in Cardiac Myocytes ? Sci Signal. 2008;25:1–5.

27. Liu Q, Molkentin JD. Protein kinase Cα as a heart failure therapeutic target Qinghang. J Mol Cell Cardiol [Internet]. 2011;51(4):474–8. Available from: http://dx.doi.org/10.1016/j.yjmcc.2010.10.004

28. Kohlhaas M, Maack C. Calcium release microdomains and mitochondria. Cardiovasc Res. 2013;98:259–68.

29. Rockman HA, Koch WJ, Lefkowitz RJ. Seven-transmembrane-spanning receptors and heart function. Nat Rev. 2002;415(January):206–12.

30. Wu X, Zhang T, Bossuyt J, Li X, Mckinsey TA, Dedman JR, et al. Local InsP3-dependent perinuclear Ca2+ signaling in cardiac myocyte excitation- transcription coupling. J Clin Invest. 2006;116(3):675–82.

31. Wilkins BJ, Molkentin JD. Calcium–calcineurin signaling in the regulation of cardiac hypertrophy. Biochem Biophys Res Commun. 2004;322:1178–91.

32. Bers DM. Cardiac excitation-contraction coupling. Nature. 2002;415:198–205.

33. Li LI, Desantiago J, Chu G, Kranias EG, Bers DM, Desantiago J, et al. Phosphorylation of phospholamban and troponin I in Beta-adrenergic-induced acceleration of cardiac relaxation. Am J Physiol Heart Circ Physiol. 2000;278:769–79.

34. Kentish JC, Mccloskey DT, Layland J, Palmer S, Leiden JM, Martin AF, et al. Phosphorylation of Troponin I by Protein Kinase A Accelerates Relaxation and Crossbridge Cycle Kinetics in Mouse Ventricular Muscle. Circ Res. 2001;88:1059–65.

35. Sei CA, Irons CE, Sprenkle AB, Mcdonough PM, Brown JH, Glembotskin CC. The alpha-Adrenergic Stimulation of Atrial Natriuretic Factor Expression in Cardiac Myocytes Requires Calcium Influx , Protein Kinase C , and Calmodulin-regulated Pathways. J Biol Chem. 1991;266(24):15910–6.

36. Ramirez MT, Zhao X, Schulman H, Brown JH. The Nuclear gama B Isoform of Ca 2 +/ Calmodulin-dependent Protein Kinase II Regulates Atrial Natriuretic Factor Gene Expression in Ventricular Myocytes. J Biol Chem. 1997;272(49):31203–8.

37. Zhu W, Zou Y, Shiojima I, Kudoh S, Aikawa R, Hayashi D, et al. Ca 2+/ Calmodulin-dependent

Kinase II and Calcineurin Play Critical Roles in Endothelin-1-induced Cardiomyocyte Hypertrophy. J Biol Chem. 2000;275(20):15239–45.

38. Backs J, Song K, Bezprozvannaya S, Chang S, Olson EN. CaM kinase II selectively signals to histone deacetylase 4 during cardiomyocyte hypertrophy. J Clin Invest. 2006;116(7):1853–64.

39. Huss JM, Kelly DP. Mitochondrial energy metabolism in heart failure : a question of balance. J Clin Invest. 2005;115(3):547–55.

40. Westermann B. Merging mitochondria matters Cellular role and molecular machinery of mitochondrial fusion. EMBO Rep. 2002;3(6):527–31.

41. Ong S, Hausenloy DJ. Mitochondrial morphology and cardiovascular disease. Cardiovasc Res. 2010;88:16–29.

42. Yu T, Sheu S-S, Robotham JL, Yoon Y. Mitochondrial fission mediates high glucose-induced cell death through elevated production of reactive oxygen species. Cardiovasc Res. 2008;79(2):341–51.

43. Pennanen C, Parra V, López-crisosto C, Pablo E, Campo A, Gutierrez T, et al. Mitochondrial fission is required for cardiomyocyte hypertrophy via a Ca 2 + -calcineurin signalling pathway. J Cell Sci. 2014;(April):1–33.

44. Wang J, Zhang X, Feng C, Sun T, Wang K, Wang Y, et al. MicroRNA-532-3p regulates mitochondrial fission through targeting apoptosis repressor with caspase recruitment domain in doxorubicin cardiotoxicity. Cell Death Dis. 2015;(38):1–11.

45. Izumo S, Nadal-ginard B, Mahdavi V. Protooncogene induction and reprogramming of cardiac gene expression produced by pressure overload. PNAS. 1988;85(January):339–43.

46. Greco CM, Condorelli G. Epigenetic modifications and noncoding RNAs in cardiac hypertrophy and failure. Nat Rev Cardiol [Internet]. 2015;12:488–97. Available from: http://dx.doi.org/10.1038/nrcardio.2015.71

47. Stein R, Gruenbaum Y, Pollack Y, Razin A, Cedar H. Clonal inheritance of the pattern of DNA methylation in mouse cells Biochemistry : PNAS. 1982;79(January):61–5.

48. Hendrich B, Tweedie S. The methyl-CpG binding domain and the evolving role of DNA methylation in animals. Trends Genet. 2003;19(5):269–77.

49. Movassagh M, Choy M, Knowles DA, Simeoni I, Penkett C, Goddard M, et al. Epigenomic Features in End-Stage Failing Human Hearts. Circulation. 2013;124(22):2411–22.

50. Wang X, Hayes JJ. Acetylation Mimics within Individual Core Histone Tail Domains Indicate Distinct Roles in Regulating the Stability of Higher-Order Chromatin Structure. Mol Cell Biol. 2008;28(1):227–36.

51. Hodawadekar S, Marmorstein R. Chemistry of acetyl transfer by histone modifying enzymes : structure , mechanism and implications for effector design. Oncogene. 2007;5528–40.

52. Zhang CL, Mckinsey TA, Chang S, Antos CL, Hill A, Olson EN. Class II Histone Deacetylases Act as Signal-Responsive Repressors of Cardiac Hypertrophy. Cell. 2015;110(4):479–88.

53. Zhang Q, Chen H, Wang L, Liu D, Hill JA, Liu Z. The histone trimethyllysine demethylase JMJD2A promotes cardiac hypertrophy in response to hypertrophic stimuli in mice. J Clin Invest. 2011;121(6):2447–56.

54. Hohl M, Wagner M, Reil J, Müller S, Tauchnitz M, Zimmer AM, et al. HDAC4 controls histone methylation in response to elevated cardiac load. J Clin Invest. 2013;123(3):1359–70.

55. Cattaneo P, Kunderfranco P, Greco C, Guffanti A, Stirparo GG, Rusconi F, et al. DOT1L-

mediated H3K79me2 modification critically regulates gene expression during cardiomyocyte differentiation. Cell Death Differ [Internet]. 2016;23(4):555–64. Available from: http://dx.doi.org/10.1038/cdd.2014.199

56. Mattick JS. The Genetic Signatures of Noncoding RNAs. PLoS Genet. 2009;5(4):e1000459.

57. Wang KC, Chang HY. Molecular mechanisms of long noncoding RNAs. Mol Cell. 2012;43(6):904–14.

58. Khalil AM, Guttman M, Huarte M, Garber M, Raj A, Rivea D, et al. Many human large intergenic noncoding RNAs associate with chromatin-modifying complexes and affect gene expression. PNAS. 2009;106(28):11667–72.

59. Wang K, Liu F, Zhou L, Long B, Yuan S, Wang Y, et al. The long noncoding RNA CHRF regulates cardiac hypertrophy by targeting miR-489. Circ Res. 2014;114:1377–88.

60. Wang K, Long B, Zhou L, Liu F, Zhou Q, Liu C, et al. CARL lncRNA inhibits anoxia-induced mitochondrial fission and apoptosis in cardiomyocytes by impairing miR-539-dependent PHB2 downregulation. Nat Commun. 2014;5:3596.

61. Han P, Li W, Lin C, Yang J, Shang C, Nuernberg ST, et al. A long noncoding RNA protects the heart from pathological hypertrophy. Nature [Internet]. 2014;514:102–6. Available from: http://dx.doi.org/10.1038/nature13596

62. Carrington JC, Ambros V. Role of MicroRNAs in Plant and Animal. Science (80-). 2003;301(336–8).

63. Van Rooij E, Sutherland LB, Liu N, Williams AH, Mcanally J, Gerard RD, et al. A signature pattern of stress-responsive microRNAs that can evoke cardiac hypertrophy and heart failure. PNAS. 2006;103(48):18255–60.

64. Sayed D, Hong C, Chen I, Lypowy J, Abdellatif M. MicroRNAs Play an Essential Role in the Development of Cardiac Hypertrophy. Circ Res. 2007;100:416–24.

65. Thum T, Galuppo P, Wolf C, Fiedler J, Kneitz S, Laake LW Van, et al. MicroRNAs in the Human Heart A Clue to Fetal Gene Reprogramming in Heart Failure. Circulation. 2007;116:258–67.

66. Flather MD, Yusuf S, Køber L, Pfeffer M, Hall A, Murray G, et al. Long-term ACE-inhibitor therapy in patients with heart failure or left-ventricular dysfunction : a systematic overview of data from individual patients. Lancet. 2000;355:1575–81.

67. Donoghue M, Hsieh F, Baronas E, Godbout K, Gosselin M, Stagliano N, et al. A Novel Angiotensin-Converting Enzyme–Related Carboxypeptidase (ACE2) Converts Angiotensin I to Angiotensin 1-9. Circ Res. 2000;87:1–9.

68. Jackman HL, Massad MG, Sekosan M, Tan F, Brovkovych V, Marcic BM, et al. Angiotensin 1-9 and 1-7 Release in Human Heart. Hypertension. 2002;39:976–81.

69. Tikellis C, Johnston CI, Forbes JM, Burns WC, Burrell LM, Risvanis J, et al. Characterization of Renal Angiotensin-Converting Enzyme 2 in Diabetic Nephropathy. Hypertension. 2003;41:392–7.

70. Ocaranza P, Godoy I, Jalil JE, Varas M, Collantes P, Pinto M, et al. Enalapril Attenuates Downregulation of Angiotensin-Converting Enzyme 2 in the Late Phase of Ventricular Dysfunction in Myocardial Infarcted Rat. Hypertension. 2006;572–8.

71. Ocaranza MP, Lavandero S, Jalil JE, Moya J, Pinto M, Novoa U, et al. Angiotensin- (1 – 9) regulates cardiac hypertrophy in vivo and in vitro. J Hypertens. 2010;28:1054–64.

72. Flores-Munoz M, Work LM, Douglas K, Denby L, Dominiczak AF, Graham D, et al.

Angiotensin- (1-9) Attenuates Cardiac Fibrosis in the Stroke-Prone Spontaneously Hypertensive Rat via the Angiotensin Type 2 Receptor. Hypertension. 2012;300–7.

73. Ocaranza MP, Moya J, Barrientos V, Alzamora R, Hevia D, Morales C. Angiotensin-(1-9) reverses experimental hypertension andcardiovascular damage by inhibition of the angiotensin converting enzyme/Ang IIaxis. J Hypertens. 2014;32:771–83.

74. Zheng H, Pu S, Fan X, Li X, Zhang Y, Yuan J, et al. Treatment with angiotensin-(1-9) alleviates the cardiomyopathy in streptozotocin-induced diabetic rats. Biochem Pharmacol [Internet]. 2015;95(1):38–45. Available from: http://dx.doi.org/10.1016/j.bcp.2015.03.009

75. Fattah C, Nather K, Mccarroll CS, Hortigon-vinagre MP, Zamora V, Flores-munoz M, et al. Gene Therapy With Angiotensin-(1-9) Preserves Left Ventricular Systolic Function After Myocardial Infarction. J Am Coll Cardiol. 2016;68(24):2652–66.

76. Mendoza-torres E, Riquelme JA, Vielma A, Sagredo AR, Gabrielli L, Bravo R, et al. Protection of the myocardium against ischemia/reperfusion injury by angiotensin-(1–9) through an AT2R and Akt-dependent mechanism. Pharmacol Res [Internet]. 2018;135:112–21. Available from: https://doi.org/10.1016/j.phrs.2018.07.022

77. Parra V, Verdejo HE, Iglewski M, Campo A, Troncoso R, Jones D, et al. Insulin Stimulates Mitochondrial Fusion and Function in Cardiomyocytes via the Akt- mTOR-NF k B-Opa-1 Signaling Pathway. Diabetes. 2014;63(February 2013):75–88.

78. Yoon Y, Krueger EW, Oswald BJ, Mcniven MA. The Mitochondrial Protein hFis1 Regulates Mitochondrial Fission in Mammalian Cells through an Interaction with the Dynamin-Like Protein DLP1. Mol Cell Biol. 2003;23(15):5409–20.

79. Cribbs JT, Strack S. Reversible phosphorylation of Drp1 by cyclic AMP-dependent protein kinase and calcineurin regulatesmitochondrial fission and cell death. EMBO Rep. 2007;8(10).

80. Parra V, Altamirano F, Hernandez-Fuentes CP, Tong D, Kyrychenko V, Rotter D, et al. Down Syndrome Critical Region 1 Gene, Rcan1, Helps Maintain a More Fused Mitochondrial Network. Circ Res. 2018;122(6):1–26.

81. Chang C-R, Blackstone C. Cyclic AMP-dependent Protein Kinase Phosphorylation of Drp1 Regulates Its GTPase Activity and Mitochondrial Morphology. J Biol Chem. 2007;282(30):21583–7.

82. Santel A, Frank S. Shaping Mitochondria : The Complex Posttranslational Regulation of the Mitochondrial Fission Protein DRP1. IUBMB Life. 2008;60(July):448–55.

83. Taguchi N, Ishihara N, Jofuku A, Oka T, Mihara K. Mitotic Phosphorylation of Dynamin-related GTPase Drp1 Participates in Mitochondrial Fission * □. J Biol Chem. 2007;282(15):11521–9.

84. Simpson P, Mcgrath A, Savion S. Myocyte Hypertrophy in Neonatal Rat Heart Cultures and Its Regulation by Serum and by Catecholamines. Circ Res. 1982;51:787–801.

85. Eisner V, Parra V, Lavandero S, Hidalgo C, Jaimovich E. Mitochondria fine-tune the slow Ca 2 + transients induced by electrical stimulation of skeletal myotubes. Cell Calcium. 2010;48(6):358–70.

86. Eisner V, Lenaers G, Hajnóczky G. Mitochondrial fusion is frequent in skeletal muscle and supports excitation–contraction coupling. J Cell Biol. 2014;205(2):179–95.

87. Gutiérrez T, Parra V, Troncoso R, Pennanen C, Contreras-ferrat A, Vasquez-trincado C, et al. Alteration in mitochondrial Ca 2 + uptake disrupts insulin signaling in hypertrophic cardiomyocytes. Cell Commun Signal. 2014;12(68):1–14.

88. Giorgi C, Stefani D De, Bononi A, Rizzuto R, Pinton P. Structural and functional link between the mitochondrial network and the endoplasmic reticulum. Int J Biochem Cell Biol.

2010;41(10):1817–27.

89. Bravo-sagua R, López-crisosto C, Parra V, Rodriguez- M, Rothermel BA, Quest AFG, et al. mTORC1 inhibitor rapamycin and ER stressor tunicamycin induce differential patterns of ER-mitochondria coupling. Sci Rep. 2016;6(36394):1–12.

90. Bravo-sagua R, Parra V, Ortiz-Sandoval C, Navarro-Marquez M, Rodriguez AE, Díaz-Valdivia N, et al. Caveolin-1 impairs PKA-DRP1-mediated remodelling of ER – mitochondria communication during the early phase of ER stress. Cell Death Differ. 2019;1:1195–212.

91. Manders EMM, J VF, Aten JA. Measurement of co-localization of objects in dual-colour confocal images. J Microsc. 1993;169(August 1992):375–82.

92. Rothermel BA, Vega RB, Williams RS. The Role of Modulatory Calcineurin-Interacting Proteins in Calcineurin Signaling. Trends Cardiovasc Med. 2003;13(1):15–21.

93. Munoz JP, Chiong M, García L, Troncoso R, Toro B, Pedrozo Z, et al. Iron induces protection and necrosis in cultured cardiomyocytes : Role of reactive oxygen species and nitric oxide. Free Radic Biol Med. 2010;48(4):526–34.

94. Chiong M, Parra V, Eisner V, Ibarra C, Maldonado C, Criollo A, et al. Parallel activation of Ca 2 + -induced survival and death pathways in cardiomyocytes by sorbitol-induced hyperosmotic stress. Apoptosis. 2010;15:887–903.

95. Contreras-Ferrat A., Toro B, Roberto B, Parra V, Ibarra C, Mears D, et al. An Inositol 1,4,5-Triphosphate (IP3)-IP3 Receptor Pathway is Required for Insulin-Stimulated Glucose Transporter 4 Translocation and Glucose Uptake in Cardiomyocytes. Endocrinology. 2010;151:4665–77.

96. Rojas-Rivera D, Díaz-Elizondo J, Parra V, Salas D, Contreras A, Toro B, et al. Regulatory volume decrease in cardiomyocytes is modulated by calcium influx and reactive oxygen species. FEBS Lett. 2009;583(21):3485–92.

97. Parra V, Eisner V, Chiong M, Criollo A, Moraga F, Jaimovich E, et al. Changes in mitochondrial dynamics during ceramide-induced cardiomyocyte early apoptosis. Cardiovasc Res. 2008;77:387–97.

98. Hasler D, Lehmann G, Murakawa Y, Rajewsky N, Landthaler M, Meister G, et al. The Lupus Autoantigen La Prevents Mis-channeling of tRNA Fragments into the Human MicroRNA Article The Lupus Autoantigen La Prevents Mis-channeling of tRNA Fragments into the Human MicroRNA Pathway. Mol Cell. 2016;63:110–24.

99. Bolger AM, Lohse M, Usadel B. Trimmomatic: A flexible trimmer for Illumina sequence data. Bioinformatics. 2014;30(15):2114–20.

100. Orell A, Tripp V, Aliaga-tobar V, Albers S, Maracaja-coutinho V, Randau L. A regulatory RNA is involved in RNA duplex formation and biofilm regulation in Sulfolobus acidocaldarius. Nucleic Acids Res. 2018;46(9):4794–806.

101. Matamala JM, Arias-carrasco R, Sanchez C, Uhrig M, Matus S, Maracaja-coutinho V, et al. Genome-wide circulating microRNA expression profiling reveals potential biomarkers for amyotrophic lateral sclerosis José. Neurobiol Aging. 2017;(2018).

102. Hubbard T, Barker D, Birney E, Cameron G, Chen Y, Clark L, et al. The Ensembl genome database project. Nucleic Acids Res. 2002;30(1):38–41.

103. Langmead B. Aligning short sequencing reads with Bowtie. Curr Protoc Bioinforma. 2010;11:1–24.

104. Quinlan AR. BEDTools : the Swiss-army tool for genome feature analysis. Curr Protoc Bioinforma. 2015;47(11):12.1-12.34.

105. Kozomara A, Birgaoanu M, Griffiths-jones S. miRBase : from microRNA sequences to function. Nucleic Acids Res. 2018;47:155–62.

106. Cunningham F, Achuthan P, Akanni W, Allen J, Amode MR, Armean IM, et al. Ensembl 2019. Nucleic Acids Res. 2019;47(November 2018):745–51.

107. Love MI, Huber W, Anders S. Moderated estimation of fold change and dispersion for RNA-seq data with DESeq2. Genome Biol. 2014;15(12):550.

108. Dueck A, Ziegler C, Eichner A, Berezikov E, Meister G. microRNAs associated with the different human Argonaute proteins. Nucleic Acids Res. 2012;40(19):9850–62.

109. Nam J, Rissland OS, Koppstein D, Abreu-goodger C, Jan CH, Agarwal V, et al. Global analyses of the effect of different cellular contexts on microRNA targeting. Mol Cell. 2015;53(6):1031–43.

110. Agarwal V, Bell GW, Nam J, Bartel DP. Predicting effective microRNA target sites in mammalian mRNAs. Elife. 2015;4(e05005):1–38.

111. Dweep H, Gretz N. miRWalk2.0: a comprehensive atlas of microRNA-target interactions. Nat Methods. 2015;8(697).

112. Harada M, Luo X, Murohara T, Yang B, Dobrev D, Nattel S. MicroRNA Regulation and Cardiac Calcium Signaling: Role in Cardiac Disease and Therapeutic Potential. Circ Res. 2014;114:689–705.

113. Rana I, Velkoska E, Patel SK, Burrell LM, Charchar FJ. MicroRNAs mediate the cardioprotective effect of angiotensin converting enzyme inhibition in acute kidney injury. Am J Physiol Ren Physiol. 2015;309:F943-54.

114. Jiang X, Ning Q, Wang J. Angiotensin II induced differentially expressed microRNAs in adult rat cardiac fibroblasts. J Physiol Sci. 2013;63:31–8.

115. Ding Y, Xu L, Jovanovic BD, Helenowski IB, Kelly DL, Catalona WJ, et al. The Methodology Used to Measure Differential Gene Expression Affects the Outcome. J Biomol Tech. 2007;18(5):321–30.

116. Menk M, Haefen C Von, Funke-kaiser H, Sifringer M, Schefe JH, Kirsch S, et al. Ethanol-induced downregulation of the angiotensin AT2 receptor in murine fibroblasts is mediated by PARP-1. Alcohol [Internet]. 2010;44(6):495–506. Available from: http://dx.doi.org/10.1016/j.alcohol.2010.05.005

117. Inuzuka T, Fujioka Y, Tsuda M, Fujioka M, Satoh AO, Horiuchi K, et al. Attenuation of ligand-induced activation of angiotensin II type 1 receptor signaling by the type 2 receptor via protein kinase C. Sci Rep [Internet]. 2016;6:1–11. Available from: http://dx.doi.org/10.1038/srep21613

118. Hwang H, Wentzel EA, Mendell JT. Cell – cell contact globally activates microRNA biogenesis. PNAS. 2009;106(17):7016–21.

119. Ding J, Li X, Hu H. TarPmiR : a new approach for microRNA target site prediction. Bioinformatics. 2016;32(May):2768–75.

120. Olsen SR, Uhler MD. Inhibition of Protein Kinase-A by Overexpression of the Cloned Human Protein Kinase Inhibitor. Mol Endocrinol. 1991;(25):1246–56.

121. Rizzuto R, Stefani D De, Raffaello A, Mammucari C. Mitochondria as sensors and regulators of calcium signalling. Mol Cell Biol [Internet]. 2012;(August). Available from: http://dx.doi.org/10.1038/nrm3412

122. Jeppesen PL, Christensen GL, Mikael S, Yaël Nossent A, Jensen Bronnum H, Andersen DC, et al. Angiotensin II type 1 receptor signalling regulates microRNA differentially in cardiac

fibroblasts and myocytes. Br J Pharmacol. 2011;164:394–404.

123. Kemp BE, Graves DJ, Krebs G. Role of Multiple Basic Residues in Determining the Substrate Specificity of Cyclic Protein Kinase *. J Biol Chem. 1977;252(14):4888–94.

124. Roeslers WJ, Vandenbark GR, Hanson RW. Cyclic AMP and the Induction of Eukaryotic Gene Transcription. J Biol Chem. 1988;263(19):9063–6.

125. Cereghetti GM, Stangherlin A, Brito OM De, Chang CR, Blackstone C, Bernardi P, et al. Dephosphorylation by calcineurin regulates translocation of Drp1 to mitochondria. PNAS. 2008;105(41):15803–8.
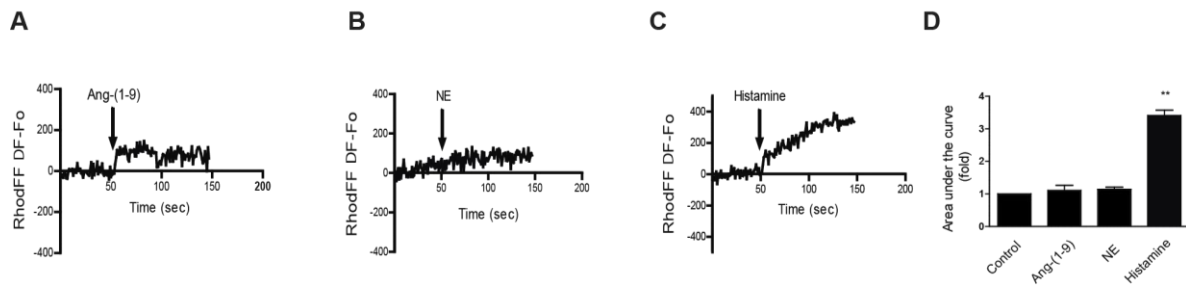
10. SUPPLEMENTARY FIGURES

A

B
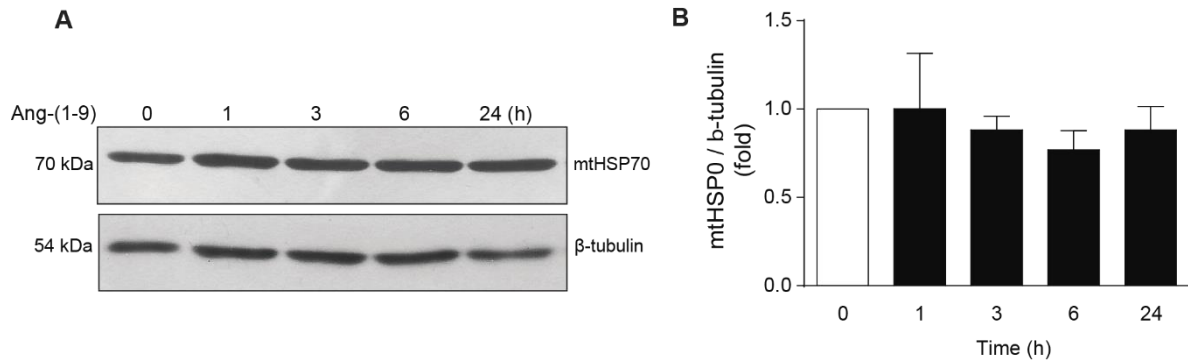
Supplementary Figure 1. Angiotensin-(1-9) promotes mitochondrial fusion without changes in total mitochondrial mass. (A) Mitochondrial chaperone mtHsp70 levels were assessed by immunoblot of cells treated with 100 μM Ang-(1-9) for the indicated times. (B) Densitometric cuantification of (A). β-tubulin was used as a loading control (n=3).

A

B

C **D** **E** **F**
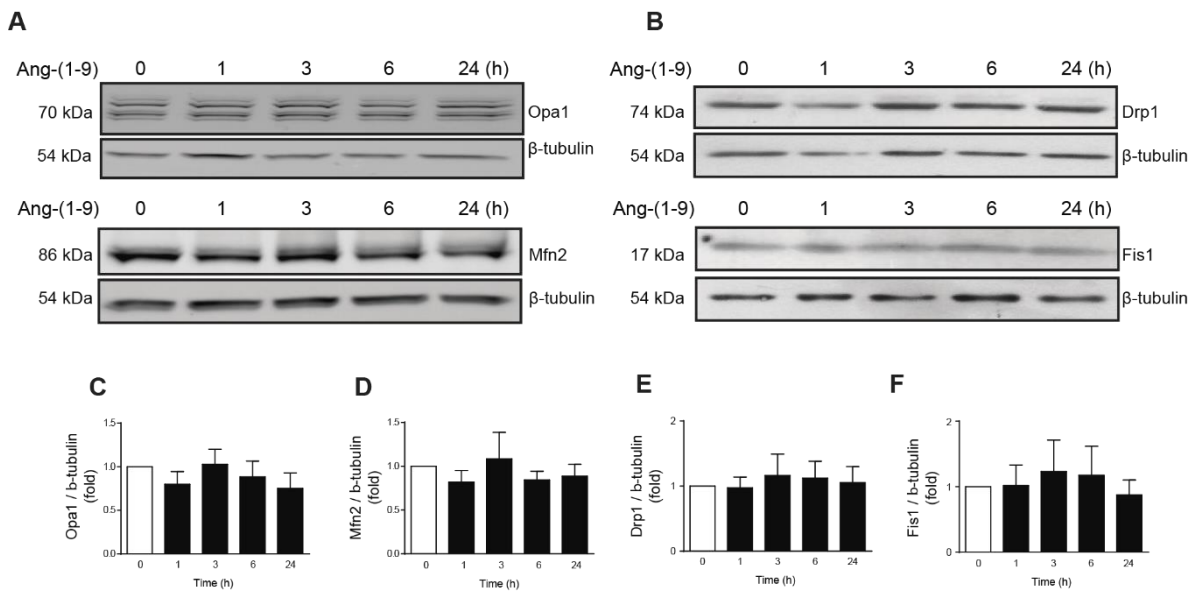
Supplementary Figure 2. Mitochondrial protein levels are not affected by Angiotensin (1-9). (A-D) Mitochondrial fusion proteins OPA1 and MFN2 and fission proteins DRP1 and FIS1. (B) Levels were assessed by Western blotting of cells treated with 100 μM angiotensin-(1-9) for the indicated times β-tubulin was used as a loading control (n=3).

79

Supplementary Figure 3 Mitochondrial calcium levels after adding different stimuli. (A-C) Angiotensin, histamine and norepinephrine pulses. (D) quantification over mitochondrial calcium mobilized.
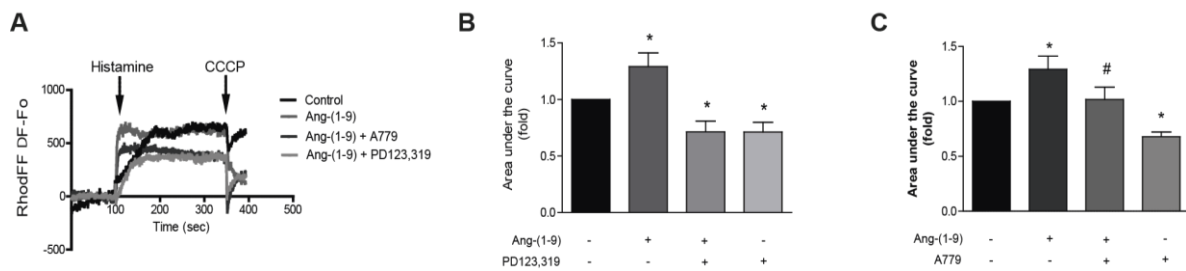
Supplementary Figure 4 Mitochondrial calcium increase induced by Angiotensin-(1-9) is blocked with AT2-R antagonist. (A) Mitochondrial Ca2+ levels in cells stimulated with angiotensin-(1-9) after pre-treatment with the AT2R or MAS antagonists PD123319 and A779 respectively. (B-C) Quantification of the area under the curve of Rhod-FF fluorescence (n=5). *p<0.05; **p<0.01; ##p<0.01 vs. angiotensin-(1-9).

A

Control

[FU]

100

50

0

25 200 1000 4000 [nt]
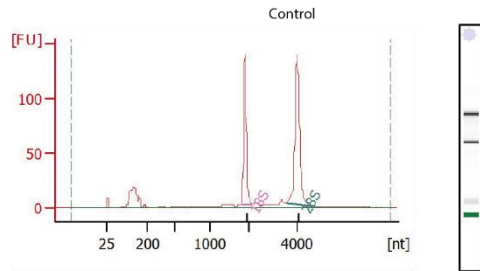
Overall Results for sample 2 : Control

RNA Area: 553.3
RNA Concentration: 5,386 pg/µl
rRNA Ratio [28s / 18s]: 1.5
RNA Integrity Number (RIN): 9.7 (B.02.08)
Result Flagging Color:
Result Flagging Label: RIN: 9.70
Fragment table for sample 2 : Control (5)

Name	Start Size [nt]	End Size [nt]	Area	% of total Area
18S	1,831	2,186	140.9	25.5
28S	3,496	4,661	215.3	38.9

B

NE

[FU]

25

20

15

10

5

0
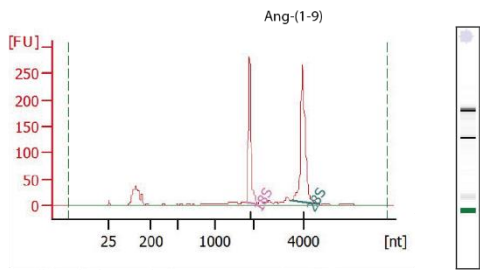
25 200 1000 4000 [nt]
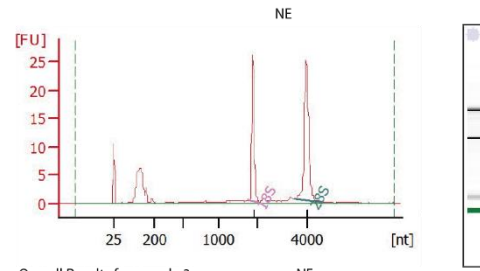
Overall Results for sample 3 : NE

RNA Area: 105.9
RNA Concentration: 1,031 pg/µl
rRNA Ratio [28s / 18s]: 1.5
RNA Integrity Number (RIN): 9.6 (B.02.08)
Result Flagging Color:
Result Flagging Label: RIN: 9.60
Fragment table for sample 3 : NE (5)

Name	Start Size [nt]	End Size [nt]	Area	% of total Area
18S	1,818	2,107	23.0	21.7
28S	3,474	4,582	35.7	33.7

C

Ang-(1-9)

[FU]

250

200

150

100

50

0

25 200 1000 4000 [nt]

Overall Results for sample 4 : Ang-(1-9)

RNA Area: 1,098.4
RNA Concentration: 10,694 pg/µl
rRNA Ratio [28s / 18s]: 1.4
RNA Integrity Number (RIN): 9.6 (B.02.08)
Result Flagging Color:
Result Flagging Label: RIN: 9.60
Fragment table for sample 4 : Ang-(1-9) (5)

Name	Start Size [nt]	End Size [nt]	Area	% of total Area
18S	1,793	2,155	278.2	25.3
28S	3,467	4,576	391.6	35.7

D

Ang-(1-9) + NE

[FU]

300

200

100

0

25 200 1000 4000 [nt]
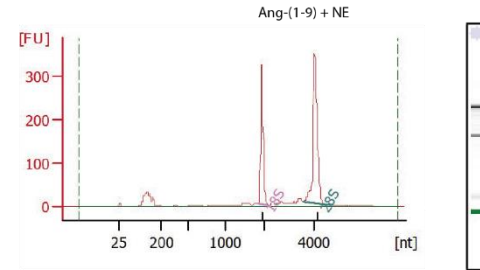
Overall Results for sample 5 : Ang-(1-9) + NE

RNA Area: 1,242.4
RNA Concentration: 12,096 pg/µl
rRNA Ratio [28s / 18s]: 1.5
RNA Integrity Number (RIN): 9.8 (B.02.08)
Result Flagging Color:
Result Flagging Label: RIN: 9.80
Fragment table for sample 5 : Ang-(1-9) + NE (5)

Name	Start Size [nt]	End Size [nt]	Area	% of total Area
18S	1,843	2,193	319.4	25.7
28S	3,544	4,678	490.8	39.5

Supplementary Figure 5 RNA integrity measurements for RNA-seq (A), (B), (C) and (D) correspond to representative quality controls for the RNA in each treatment condition before library pooling. Each replicate (n=5) in each condition was evaluated using a bioanalyzer (Agilent Technologies).
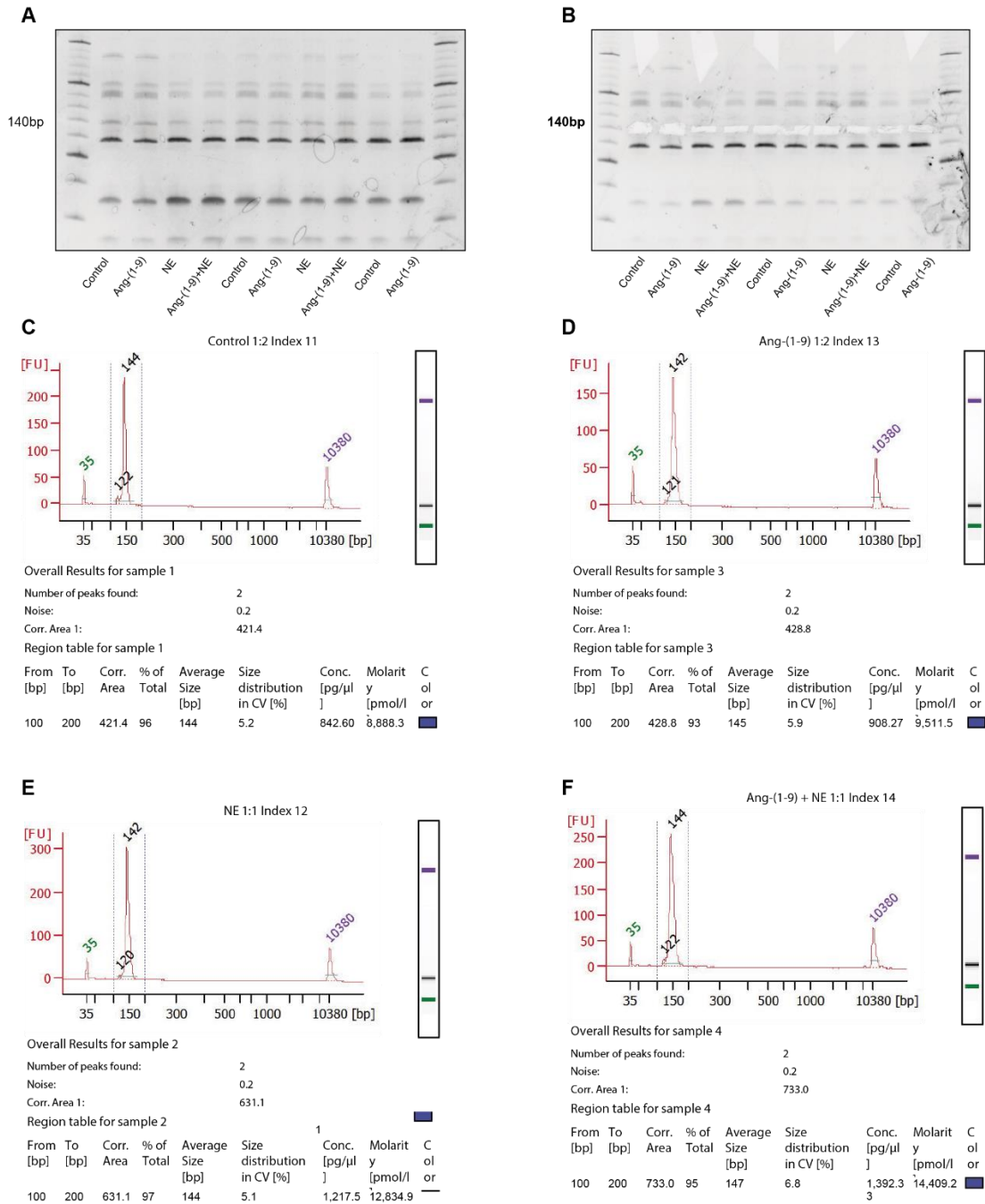
Supplementary Figure 6. Library pool quality assessment for RNA-seq (A) Representative image from run samples on 6% polyacrylamide (acrylamide/bisacrylamide 19:1) urea gel (National Diagnostics); (B) Bands were cut at the corresponding PCR amplification products containing miRNA-sized inserts; (C), (D), (E), (F) are representative electropherograms of the quality assessment for each treatment, also evaluated using a bioanalyzer (Agilent Technologies). Each replicate (n=5) in each condition was evaluated to confirm quality and concentration to obtain the library pool.